iScience

CellPress
OPEN ACCESS

Article

Kinesin-2 motors differentially impact biogenesis of extracellular vesicle subpopulations shed from sensory cilia

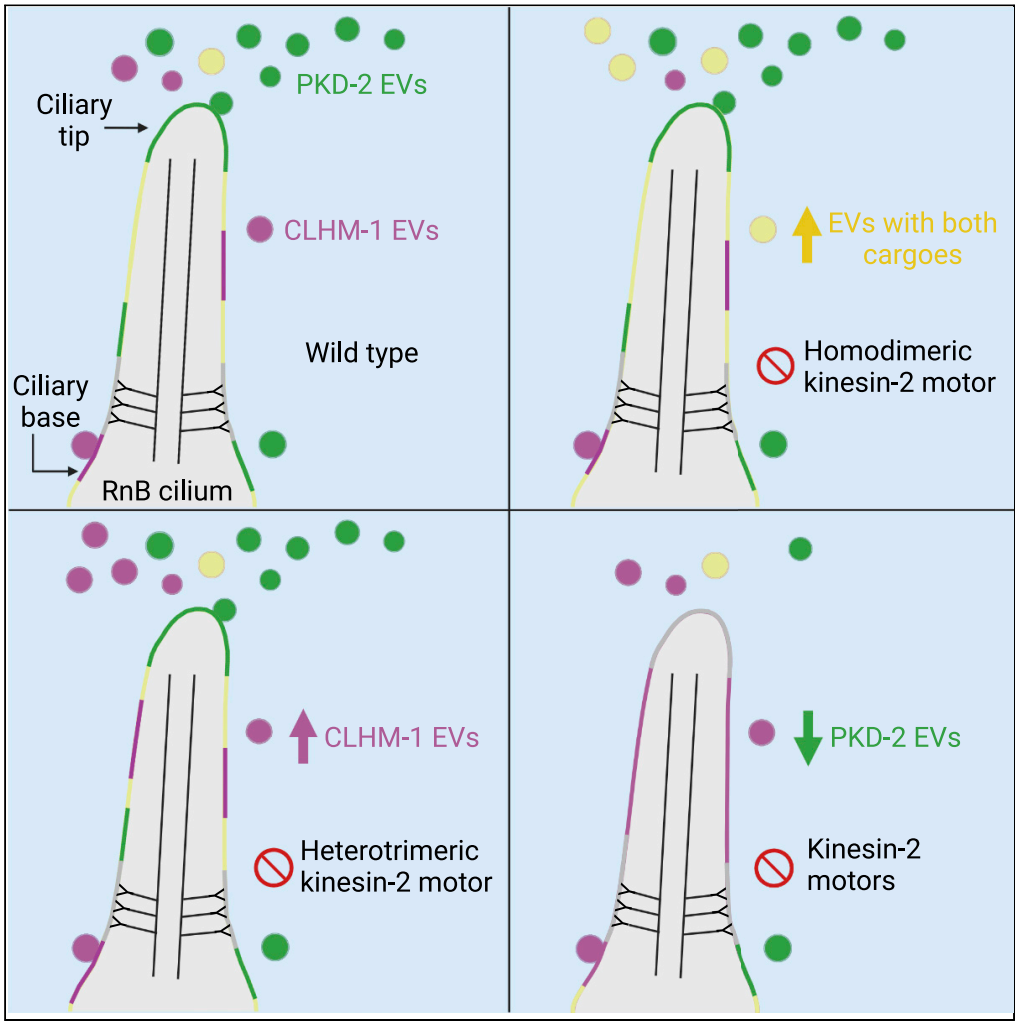

Michael Clupper, Rachael Gill, Malek Elsayyid, Denis Touroutine, Jeffrey L. Caplan, Jessica E. Tanis

jtanis@udel.edu

Highlights

The ion channel CLHM-1 is a cargo in cilia-derived EVs

Heterogeneous EV subpopulations are differentially shed in response to mate presence

Individual kinesin motors regulate EV cargo enrichment, biogenesis, and release

Kinesin-2 motors are not required for EV shedding from the ciliary base

Clupper et al., iScience 25, 105262
November 18, 2022
https://doi.org/10.1016/j.isci.2022.105262

iScience

CellPress
OPEN ACCESS

Article

Kinesin-2 motors differentially impact biogenesis of extracellular vesicle subpopulations shed from sensory cilia

Michael Clupper,[1] Rachael Gill,[1,3] Malek Elsayyid,[1,3] Denis Touroutine,[1] Jeffrey L. Caplan,[1,2] and Jessica E. Tanis[1,4,*]

SUMMARY

Extracellular vesicles (EVs) are bioactive lipid-bilayer enclosed particles released from nearly all cells. One specialized site for EV shedding is the primary cilium. Here, we discover the conserved ion channel CLHM-1 as a ciliary EV cargo. Imaging of EVs released from sensory neuron cilia of *Caenorhabditis elegans* expressing fluorescently tagged CLHM-1 and TRP polycystin-2 channel PKD-2 shows enrichment of these cargoes in distinct EV subpopulations that are differentially shed in response to mating partner availability. PKD-2 alone is present in EVs shed from the cilium distal tip, whereas CLHM-1 EVs bud from a secondary site(s), including the ciliary base. Heterotrimeric and homodimeric kinesin-2 motors have discrete impacts on PKD-2 and CLHM-1 colocalization in both cilia and EVs. Total loss of kinesin-2 activity decreases shedding of PKD-2 but not CLHM-1 EVs. Our data demonstrate that anterograde intraflagellar transport is required for selective enrichment of protein cargoes into heterogeneous EVs with different signaling potentials.

INTRODUCTION

Nearly all cells release extracellular vesicles (EVs), which mediate the intercellular transport of biological macromolecules. These lipid bilayer enclosed vesicles are typically categorized as either exosomes, which arise from the endosomal recycling pathway, or ectosomes, which are shed directly from the plasma membrane (O'Brien et al., 2020; van Niel et al., 2018). Dictated by cell of origin, EV cargoes play active roles in regulating physiological processes and propagating pathological conditions (Gassama and Favereaux, 2021; Lane et al., 2018; Yáñez-Mó et al., 2015). A single cell can release multiple discrete subpopulations of both exosomes and ectosomes, which are enriched with different molecular cargoes and have distinct physiological functions (Kowal et al., 2016; Wang and Lu, 2017). Questions remain regarding how cells enrich specific cargoes into EVs to foster this heterogeneity.

Bioactive EVs are shed from primary cilia (Nager et al., 2017; Phua et al., 2017; Wang et al., 2014; Wood et al., 2013), highly conserved microtubule-based organelles that protrude from most eukaryotic cells to provide a platform for organizing both signal transduction (Delling et al., 2013; Jiang et al., 2019; Loktev and Jackson, 2013; Wheway et al., 2018) and signal transmission (Volz et al., 2021; Wang et al., 2014; Wang and Barr, 2016; Wood et al., 2013). The protein composition of primary cilia is dynamically mediated by intraflagellar transport (IFT), which employs microtubule binding motor proteins and cargo adaptor proteins to translocate signaling components along the ciliary ultrastructure (Blacque et al., 2004; Kobayashi et al., 2020; Prevo et al., 2017; Qin et al., 2005; Singh et al., 2020). Certain IFT components play a role in ciliary EV shedding and release (Akella et al., 2020; Nager et al., 2017; O'Hagan et al., 2017, Wang et al., 2021, 2014), although the specific contribution of individual IFT motor proteins to selective cargo enrichment is unclear.

In *Caenorhabditis elegans*, EVs are shed from primary cilia of select sensory neurons, including the inner labial type 2 (IL2) neurons, as well as the male-specific ray type B (RnB), hook B (HOB), and cephalic male (CEM) neurons (Wang et al., 2014). Collectively, these neurons are referred to as the EV-releasing neurons (EVNs) (Wang et al., 2015). EVs shed from the ciliary distal tip of male-specific EVNs are released through a cuticular pore into the environment and are deposited at the hermaphrodite vulva during copulation (Wang et al., 2021, 2020) and can modulate animal behavior (Wang et al., 2014). Conversely, EVs shed

[1]Department of Biological Sciences, University of Delaware, Newark, DE 19716, USA

[2]Department of Plant and Soil Sciences, University of Delaware, Newark, DE 19716, USA

[3]These authors contributed equally

[4]Lead contact

*Correspondence: jtanis@udel.edu

https://doi.org/10.1016/j.isci.2022.105262

from the periciliary membrane compartment (PCMC) at the ciliary base can be phagocytosed by adjacent glial cells to help maintain cilia structure and function (Razzauti and Laurent, 2021; Wang et al., 2021). Very few ciliary EV cargo proteins have been examined in detail (Nikonorova et al., 2022), limiting our understanding of mechanisms underlying cargo enrichment into these EVs.

Here, we identified the ion channel CLHM-1 in EVs released from both male and hermaphrodite ciliated sensory neurons. In the absence of mating partners, release of CLHM-1-containing EVs from males decreased, suggesting that this process is a physiological response to mate availability. Visualizing EVs containing different fluorescently labeled cargoes, we discovered that discrete ciliary localization of CLHM-1 resulted in enrichment in an environmentally released EV subpopulation distinct from previously described EVs. Loss of individual kinesin-2 motors had differential impact on protein colocalization in cilia and EVs. Unlike other known EV cargoes, complete elimination of kinesin-2 motor protein activity did not inhibit CLHM-1 cilia entry or inclusion in EVs. Our results highlight CLHM-1 as a unique *C. elegans* ciliary EV cargo and demonstrate that anterograde IFT is a selective mechanism for cargo enrichment.

RESULTS

CLHM-1 is cargo in EVs released from *C. elegans* sensory neuron cilia

Calcium homeostasis modulator 1 (*CALHM1*) is an ion channel that modulates neuron excitability (Ma et al., 2012; Vingtdeux et al., 2016), and human genetic studies suggest that the P86L polymorphism in *CALHM1* lowers the age of Alzheimer's disease onset (Dreses-Werringloer et al., 2008; Lambert et al., 2010). CALHM1 and its sole *C. elegans* homolog, CLHM-1, exhibit similar biophysical properties and functional conservation (Tanis et al., 2013, 2017). *clhm-1* was found to be expressed in a subset of ciliated neurons, including the six IL2s, the left and right ASE, ASG, ASI, ASJ, ASK, ADE neurons, and the left and right phasmid A and B neurons (Figure 1A) (Tanis et al., 2013). To determine if *clhm-1* is also expressed in male-specific neurons, we created transgenic animals coexpressing *gfp* from the *clhm-1* promoter and *mCherry* from the *klp-6* promoter, which drives expression in IL2 and male ciliated sensory neurons (Peden and Barr, 2005). Colocalization analysis showed that *clhm-1* is expressed in the four CEM neurons in the male head, the HOB, and all RnB neurons in the male tail (Figure 1A), which shed EVs (Figure 1B) (Akella et al., 2020; Nikonorova et al., 2022, Wang et al., 2021, 2015, 2014).

To define CLHM-1 neuronal localization, we coexpressed tdTomato (tdT)-tagged CLHM-1 with GFP-tagged KLP-6 and observed CLHM-1 in the PCMC of the ciliary base and middle segment of the cilium proper (Figures 1C and 1D). We confirmed this localization pattern by coexpression of CLHM-1:tdT with mNeonGreen (mNG)-tagged MKS-2 (Figure 1E), a core protein of the Meckel syndrome (MKS) module that localizes exclusively to the cilium transition zone (Lange et al., 2021; Li et al., 2016). Based on the localization of CLHM-1 to the cilia of multiple EVNs and the permeability of CALHM channels to Ca^{2+} and ATP (Demura et al., 2020; Ma et al., 2012, 2018; Tanis et al., 2013; Taruno et al., 2013), both of which play a role in EV shedding (Lombardi et al., 2021; Nabhan et al., 2012; Taylor et al., 2020), we hypothesized that CLHM-1 could regulate EV biogenesis. To test this, we crossed GFP-tagged PKD-2, a conserved TRP polycystin-2 channel and well-characterized cargo present in cilia tip-derived EVs (Wang et al., 2021; 2020, 2014), with *clhm-1(tm4071)*. Loss of *clhm-1* had no effect on the number of PKD-2 containing EVs released into the environment (Figure 1F). This suggests that CLHM-1 is not required for release of these ciliary EVs under basal conditions.

We next considered that CLHM-1 could be packaged into ciliary EVs. Using structured illumination and total internal reflection fluorescence (TIRF) microscopy, we imaged animals expressing CLHM-1:GFP at single copy and discovered that CLHM-1 is cargo in EVs released from male tail EVNs (Figures 1G and 1H). Using lambda spectral imaging followed by linear unmixing, we confirmed the signal from EVs as bona fide GFP emission (Figure S1). Of interest, CLHM-1:GFP EV release was not restricted to males, and also observed from hermaphrodites (Figures 1I–1K). Because CLHM-1 tagged with GFP is functional and expressed at single copy levels (Tanis et al., 2013), this localization to EVs is not the result of aberrant protein folding or over-expression. Furthermore, not all ciliary localized proteins in these neurons are found in EVs (Wang et al., 2021; 2015, 2014), indicating that CLHM-1 is selectively packaged.

CLHM-1 and PKD-2 cargoes are enriched in distinct EV subpopulations

Expression of PKD-2 is restricted to male-specific neurons, whereas CLHM-1 is expressed in a wider subset of both male and hermaphrodite ciliated sensory neurons (Barr et al., 2001; Tanis et al., 2013). Although we

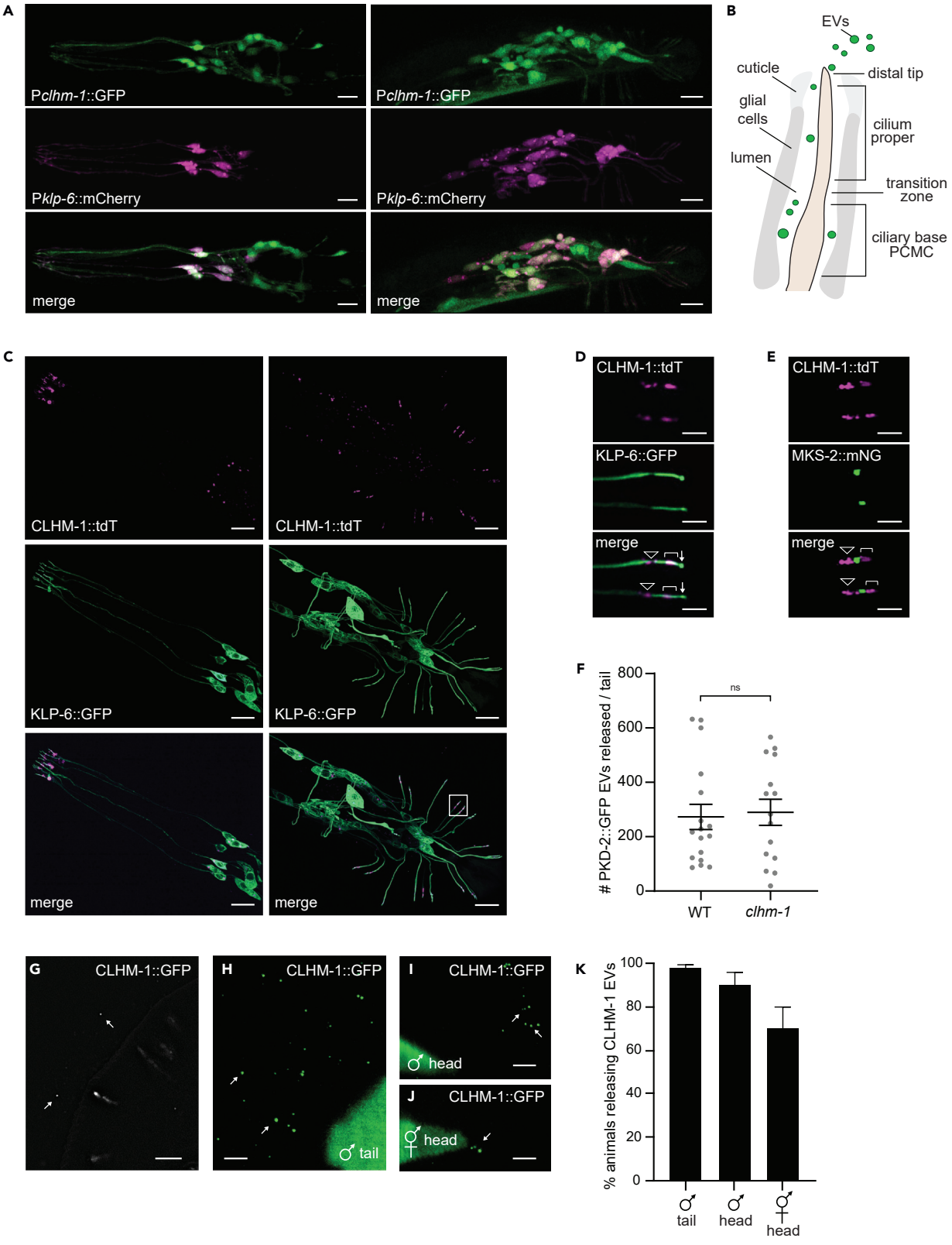
A
Pclhm-1::GFP
Pklp-6::mCherry
merge
B
EVs
cuticle
distal tip
glial cells
cilium proper
lumen
transition zone
ciliary base PCMC
C
CLHM-1::tdT
KLP-6::GFP
merge
D
CLHM-1::tdT
KLP-6::GFP
merge
E
CLHM-1::tdT
MKS-2::mNG
merge
F
PKD-2::GFP EVs released / tail
800
600
400
200
0
ns
WT
clhm-1
G
CLHM-1::GFP
H
CLHM-1::GFP
tail
I
CLHM-1::GFP
head
J
CLHM-1::GFP
head
K
% animals releasing CLHM-1 EVs
100
80
60
40
20
0
tail
head
head

Figure 1. CLHM-1 is cargo in EVs released from male and hermaphrodite ciliated neurons

(A) A P*clhm-1:gfp* transgene (top) drives GFP expression in male head (left) and tail (right) neurons. Colocalization with a P*klp-6:mCherry* reporter (middle) shows that *clhm-1* is expressed in IL2, CEM, RnB, and HOB EVNs (merge, bottom) plus additional sensory neurons. Scale bars, 10 μm.

(B) Schematic of EVs released from a *C. elegans* cilium into the environment.

(C) CLHM-1:tdT (top) localizes to neuronal cilia in the adult male head (left) and tail (right). EVNs are filled out with KLP-6:GFP (middle). Bottom, merge; scale bars, 10 μm.

(D) CLHM-1 localizes to the ciliary base (triangle) and cilium proper (bracket), but is excluded from the distal tip (arrow); R4B and R5B (box, panel C); scale bars, 3 μm.

(E) CLHM-1:tdT (top) is excluded from the transition zone, labeled with MKS-2:mNG (middle) in R4B and R5B cilia. Labels and scale as in (D).

(F) Average number of PKD-2:GFP EVs released from the male tail does not change between wild type and *clhm-1(tm4071)* animals. Data are represented as mean ± SEM, Mann-Whitney test; n ≥ 15.

(G) Structured illumination microscopy shows CLHM-1:GFP localized to RnB cilia and released in EVs (arrows). Scale bar, 5 μm.

(H–J) TIRF microscopy shows CLHM-1:GFP EVs (arrows) released from the male tail (H), male head (I), and hermaphrodite head (J). Scale bars, 3 μm.

(K) Percent of males and hermaphrodites releasing CLHM-1 EVs. n ≥ 23 animals. See also Figure S1.

observed release of CLHM-1:GFP EVs from nearly every animal of both sexes, fewer EVs were detected in images of males expressing CLHM-1:GFP compared to those expressing PKD-2:GFP. As a single cilium can release multiple EV subpopulations (Nikonorova et al., 2022; Wang et al., 2021), we hypothesized that CLHM-1 could be enriched in a different environmentally released EV subset than PKD-2. We created animals expressing single-copy insertion (SCI) fluorescent transgenes in a high incidence of males *him-5(e1490)* background (Hodgkin et al., 1979): one strain coexpressing CLHM-1:GFP with CLHM-1:tdT, a second strain coexpressing PKD-2:GFP with PKD-2:tdTomato, and two strains coexpressing PKD-2:GFP with CLHM-1:tdT. Using TIRF microscopy, we imaged EVs released from male tail EVNs, as these EVs are abundant and are deposited on the hermaphrodite vulva during mating, indicating physiological potential (Nikonorova et al., 2022; Wang et al., 2020). Transgene expression was driven by appropriate promoters to ensure overlap in the tail EVNs. CLHM-1:GFP largely colocalized with CLHM-1:tdT in environmentally-released EVs (Figure 2A), as did PKD-2:GFP and PKD-2:tdTomato (Figure 2B). In contrast, CLHM-1:tdT and PKD-2:GFP were observed together in fewer EVs (Figure 2C).

Using the Imaris spot detector, calibrated to minimize noise detection whilst maximizing signal detection, we identified EVs with GFP or tdTomato signal, as well as EVs with signal overlap (Figure S2). The number of environmentally-released EVs containing CLHM-1 was not different between strains carrying *henSi2* or *henSi17*, two different SCI CLHM-1:tdT transgenes (Figure 2D). In addition, pairing a CLHM-1:tdT transgene with a CLHM-1:GFP SCI transgene (*drSi33*) or two different PKD-2:GFP SCI transgenes (*henSi20* and *henSi21*) did not alter the number of CLHM-1:tdT EVs detected (Figure 2D). This shows that the presence of GFP-labeled CLHM-1 does not alter the number of detectable CLHM-1:tdT EVs and demonstrates that our imaging and analysis pipeline generates reproducible quantitative data with multiple independent transgenes.

We next examined signal overlap in EVs and discovered that CLHM-1:GFP was significantly more likely than PKD-2:GFP to colocalize with CLHM-1:tdT, despite PKD-2:GFP being the more abundant EV cargo (Figure 2E). Likewise, PKD-2:tdTomato was significantly more likely than CLHM-1:tdT to colocalize with PKD-2:GFP in EVs (Figure 2F). These data indicate that PKD-2 and CLHM-1 are deliberately enriched into distinct subpopulations of EVs shed from the same sensory neuron cilia.

Mating partner presence differentially impacts release of PKD-2 and CLHM-1 containing EVs

Given the observation of CLHM-1 and PKD-2 in distinct EV subpopulations, we wondered if these EVs were differentially shed in response to environmental cues. The presence of hermaphrodite mating partners has been shown to modulate relative abundance of PKD-2-containing EVs (Wang et al., 2021). We compared the number of CLHM-1:tdT-containing EVs shed from tail sensory neurons of males cultured with adult hermaphrodites to the number released by virgin males separated from hermaphrodites at the fourth larval (L4) stage. The absence of mating partners significantly reduced CLHM-1 EV release (Figure 3A). Conversely, release of PKD-2 EVs from virgin males was significantly higher compared to males cultured with hermaphrodites (Figures 3B and S3). We observed a significant increase in the probability of PKD-2:GFP being present in CLHM-1:tdT EVs released from virgin adult males, possibly because of the concurrent increase in PKD-2 and decrease in CLHM-1 EV shedding (Figure 3C).

Male tail neurons respond to mechanosensory cues, while many head EVNs are chemosensory (Johnson et al., 2017; Liu and Sternberg, 1995; White et al., 2007). Thus, we sought to determine if mating partner

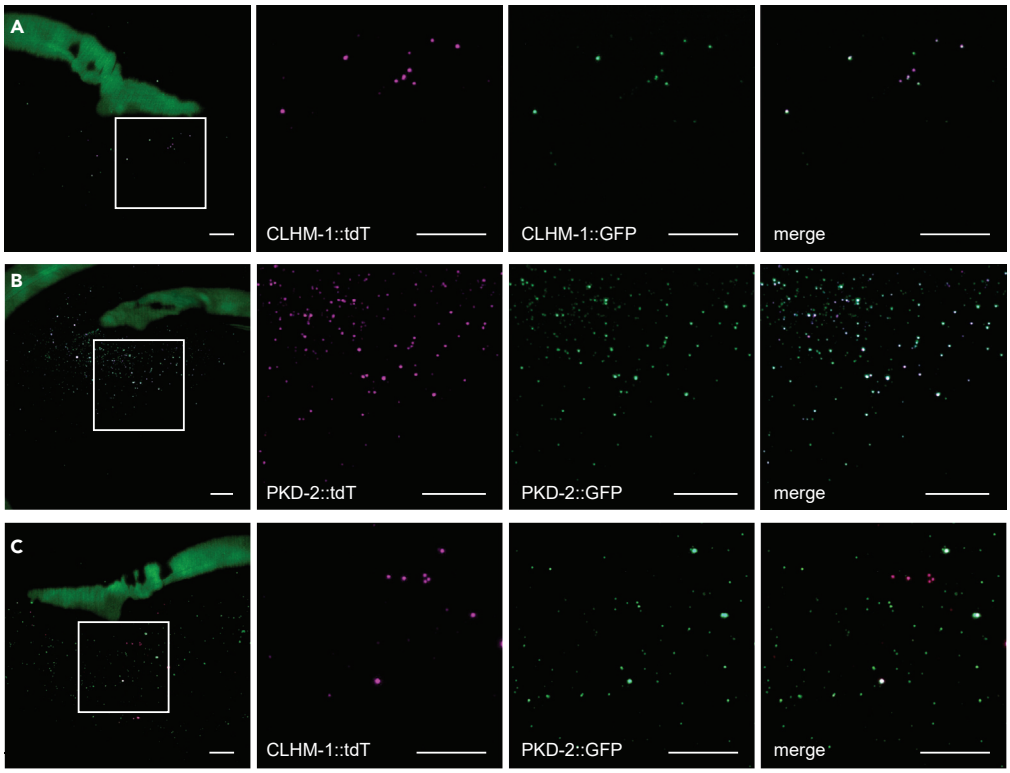

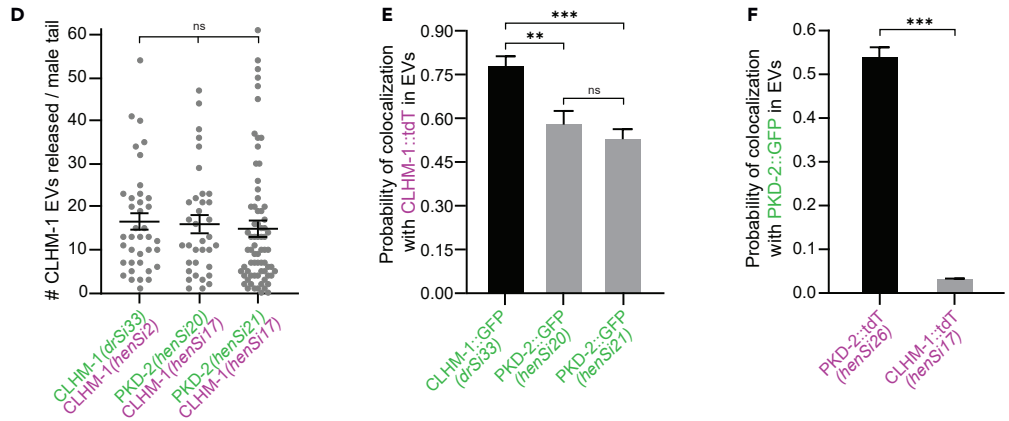

Figure 2. CLHM-1 and PKD-2 are enriched in distinct EV subpopulations released from male tail EVNs

(A) CLHM-1:tdT (*henSi2*) and CLHM-1:GFP (*drSi33*) colocalize in EVs released into the environment. Boxed region (left) is enlarged in subsequent images to clearly show EVs.

(B) PKD-2:tdT (*henSi26*) and PKD-2:GFP (*henSi20*) colocalize in EVs.

(C) PKD-2:GFP (*henSi20*) and CLHM-1:tdT (*henSi17*) display less frequent colocalization in EVs (compare to A,B).

(D) Average number of CLHM-1:tdT EVs released is not different between animals expressing different CLHM-1:tdT transgenes (*henSi2, henSi17*) or when CLHM-1:tdT is paired with different PKD-2:GFP SCI transgenes (*henSi20, henSi21*); n $\geq$ 35 animals.

(E) Probability of GFP cargo colocalization with CLHM-1:tdT in EVs. CLHM-1:GFP is more likely than PKD-2:GFP to coincide with CLHM-1:tdT; n $\geq$ 35 animals.

(F) Probability of tdTomato cargo colocalization with PKD-2:GFP in EVs. PKD-2:tdT is more likely than CLHM-1:tdT to coincide with PKD-2:GFP; n $\geq$ 29 animals. Scale bars, 10 μm. Data are represented as mean ± SEM. Kruskal-Wallis test used for (D,E). Mann-Whitney test used for (F). ** = p<0.01, *** = p<0.001. See also Figure S2.

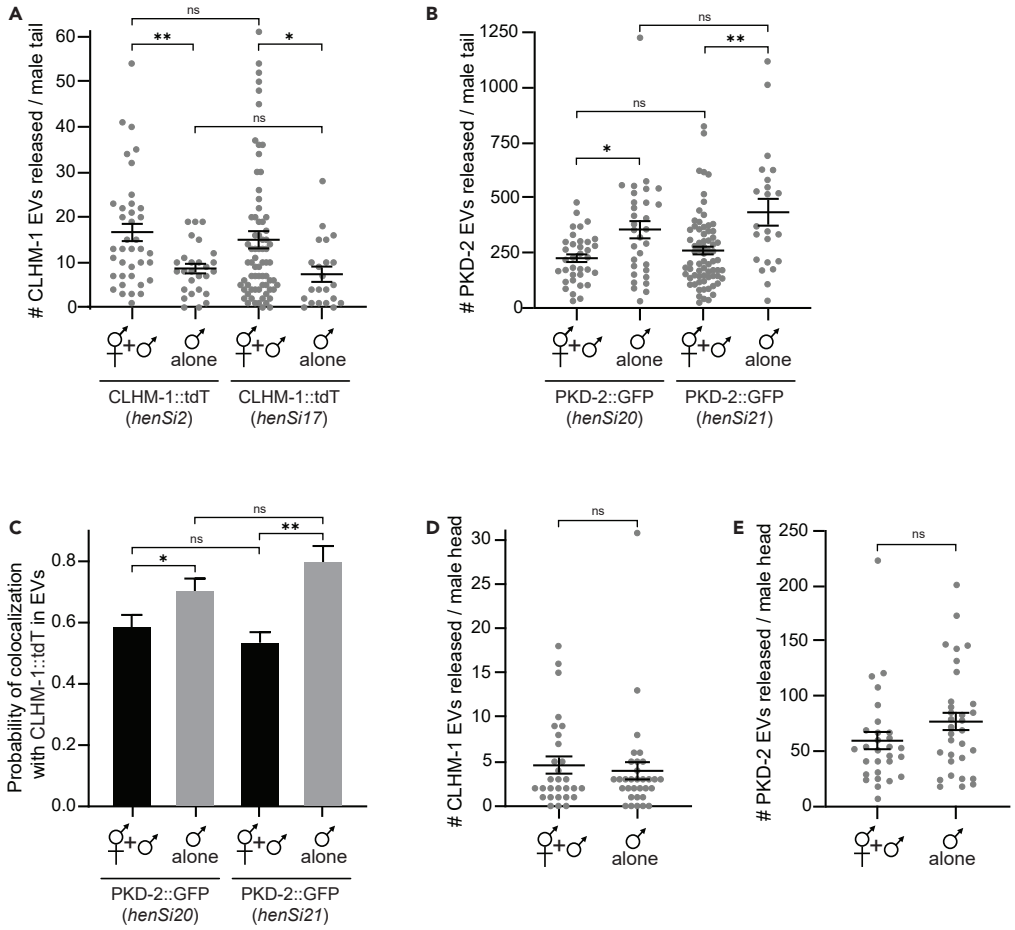

Figure 3. Abundance of CLHM-1 and PKD-2 containing EVs is dependent on mating partner availability

(A) Average number of CLHM-1:tdT EVs released per virgin male tail is lower compared to males raised with mating partners, consistent between transgenes (*henSi2, henSi17*); n ≥ 22.

(B) Average number of PKD-2:GFP EVs released per virgin male tail is higher compared to males raised with mating partners, consistent between transgenes (*henSi20, henSi21*); n ≥ 22.

(C) Probability of PKD-2:GFP being present in a CLHM-1:tdT-containing EV is greater in EVs released from virgin male tails compared to males raised with mating partners; n ≥ 20.

(D) Availability of mating partners does not affect release of CLHM-1:tdT (*henSi17*) EVs from the male head; n ≥ 29.

(E) Average number of PKD-2:GFP (*henSi21*) EVs released per virgin adult male head is not statistically different compared to males raised with mating partners; n ≥ 29. Data are represented as mean ± SEM; Mann-Whitney test * = p<0.05, ** = p<0.01. See also Figure S3.

availability had differential impact on EV release from neurons that respond to different stimuli. Hermaphrodite presence caused similar trends in EV release from male head EVNs as observed for the tail neurons; however, the data were not statistically significant (Figures 3D and 3E). This suggests that the presence of mating partners does not affect EV shedding from male head EVNs or, because fewer EVs are shed from these neurons, small changes in release may be more difficult to quantitate (Figures 3E and S3). Nevertheless, CLHM-1 and PKD-2 EV release, at least from tail EVNs, is differentially altered by mating partner availability. This demonstrates that cargo abundance within these EVs is a dynamically regulated and not just the result of non-specific ciliary membrane shedding.

PKD-2, but not CLHM-1, localizes to the distal segment of male tail EVN cilia

Primary cilia contain multiple distinct compartments, each with unique ultrastructure, protein enrichment and lipid composition (Jensen et al., 2015). In *C. elegans* EVNs, the distal dendrite gives way to a specialized PCMC at the ciliary base and the transition zone separates the ciliary base from the cilium proper

(Blacque and Sanders, 2014; Doroquez et al., 2014; Jensen et al., 2015; Kaplan et al., 2012; Silva et al., 2017). Although both PKD-2 and CLHM-1 are ciliary proteins (Barr et al., 2001; Tanis et al., 2013), we reasoned that enrichment of these cargoes in distinct EV subpopulations could result from differential localization to specific ciliary compartments.

To define relative CLHM-1 and PKD-2 localization, we imaged RnB neurons in males coexpressing CLHM-1:tdT with PKD-2:GFP. Although both CLHM-1 and PKD-2 localized to the PCMC and middle segment of the cilium proper, PKD-2:GFP alone extended into the distal tip (Figures 4A and 4B). We quantified colocalization between CLHM-1:tdT and either CLHM-1:GFP or PKD-2:GFP in three-dimensional RnB cilia reconstructions. The Manders 1 (M1) colocalization coefficient, a measure of green pixels that co-occur with red pixels, was higher in the cilium proper when comparing overlap of CLHM-1:GFP with CLHM-1:tdT to overlap of PKD-2:GFP with CLHM-1:tdT (Figure 4C). We also analyzed PKD-2:GFP and CLHM-1:tdT fluorescence intensity along the cilia in two-dimensional image projections. Distribution profiles showed that PKD-2:GFP extended into the distal tip whereas CLHM-1:tdT was absent, consistent with our visual observations and three-dimensional analyses (Figure 4D). We frequently observed EVs containing only PKD-2 being shed from the distal tip (Figure 4E) as previously described (Wang et al., 2021). Thus, the absence of CLHM-1 from this ciliary subcompartment provides an opportunity for enrichment of PKD-2 cargo into one EV subpopulation.

We observed regions in the cilium middle segment and PCMC that contained only tdTomato signal (Figure 4B) that cannot be described by the M1 coefficient, which only provides colocalization information for pixels containing GFP. The Manders 2 (M2) coefficient, which indicates the percentage of red pixels that co-occur with green pixels, was lower in the cilium proper of animals that expressed CLHM-1:tdT with PKD-2:GFP compared to CLHM-1:GFP, suggesting that regions of the cilium proper contain CLHM-1 but not PKD-2 (Figure 4F). Both M1 and M2 colocalization coefficients were also lower in the PCMC when CLHM-1:tdT was coexpressed with PKD-2:GFP compared to CLHM-1:GFP (Figures 4G and 4H). These data suggest that although these two ion channels do colocalize in the cilia, there exist regions in both the cilium proper and PCMC that contain CLHM-1, but not PKD-2.

Because our data demonstrate that CLHM-1-containing EVs are not tip-derived yet are still released into the environment, these EVs must originate from a secondary site(s). We often observed shedding of CLHM-1 EVs from the PCMC (Figures 4A and 4I–4L). It remains possible that CLHM-1 EVs also bud from the cilium proper. However, we were unable to determine if EVs adjacent to the middle segment were shed from the PCMC, then moving toward the environment for release, or if they were directly shed from the cilium proper. (Figure 4J). In conclusion, we suggest that enrichment of CLHM-1 and PKD-2 into discrete subpopulations of EVs derived from multiple sites on the same cilium is achieved by differential ciliary localization (Figure 4M).

Kinesin-2 motors specify EV cargo enrichment and biogenesis

IFT, the bidirectional movement of proteins along ciliary microtubules, is required for establishing and maintaining cilium ultrastructure and compartmentalization (Prevo et al., 2017). Anterograde IFT in *C. elegans* cilia is driven by members of the kinesin-2 family; homodimeric kinesin OSM-3 and a heterotrimeric kinesin comprised of KLP-11, KLP-20, and KAP-1 (Pan et al., 2006; Snow et al., 2004). In IL2 and male-specific EVNs, the kinesin-3 KLP-6 also participates in anterograde IFT (Morsci and Barr, 2011). As IFT is required for translocation of many ciliary membrane proteins, we considered that this could serve as a mechanism to enrich PKD-2 and CLHM-1 into different ciliary regions and thus, EV subpopulations.

We found that the average number of PKD-2:GFP EVs released from male tail EVNs did not change between wild type, *osm-3(mn391)*, *osm-3(p802)*, and *klp-11(tm324)* mutants (Figure 5A). Analysis of ciliary PKD-2:GFP distribution showed that PKD-2 was still transported to the RnB distal tip in both *klp-11* and *osm-3* mutants (Figures 5B and 5C), consistent with lack of impact of these mutations on EV release. Surprisingly, loss of either *osm-3* or *klp-11* significantly increased release of EVs containing CLHM-1 (Figure 5D) without impacting CLHM-1:tdT ciliary distribution (Figures 5B and 5C). Loss of either *osm-3* or *klp-11* did not affect average CLHM-1:tdT intensity in the cilium proper, but did cause a small decrease in fluorescence intensity in the PCMC, possibly the result of increased CLHM-1:tdT EV shedding from this compartment (Figures 5E and 5F). Together, these results suggest that the kinesin-dependent increase in CLHM-1-containing EV shedding is not a result of ciliary mislocalization.

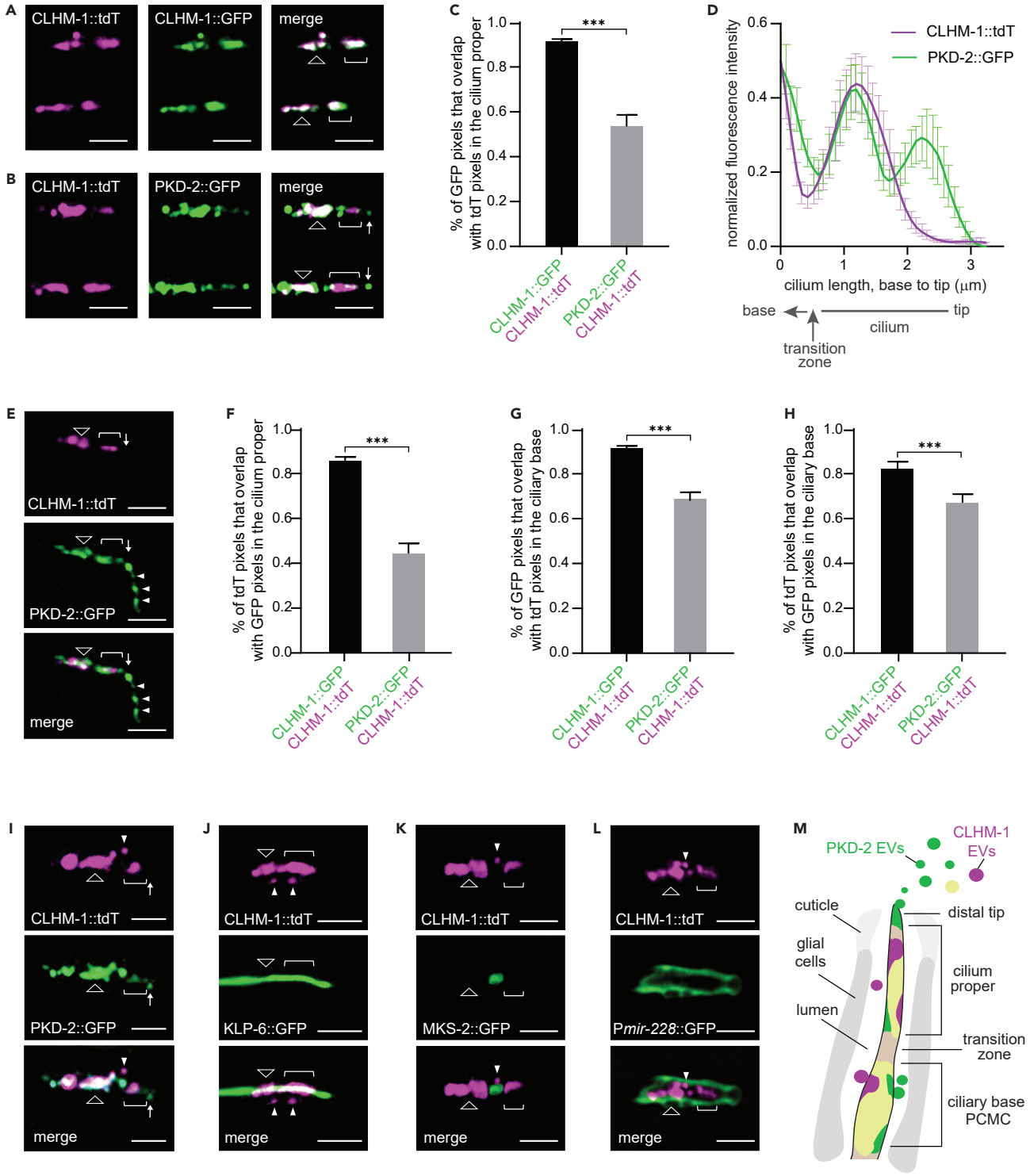

Figure 4. EVs released into the environment are shed from multiple ciliary subcompartments

(A) CLHM-1:tdT (left) and CLHM-1:GFP (middle) localize to the ciliary base (triangle) and the middle segment (bracket). Representative R4B and R5B cilia shown; scale bars, 2 μm.

(B) CLHM-1:tdT (left) and PKD-2:GFP (middle) colocalize in the ciliary base (triangle) and middle segment (bracket). PKD-2:GFP localizes to the distal tip (arrow) of R4B and R5B cilia; scale bars, 2 μm.

(C) In the cilium proper, the M1 colocalization coefficient is higher when CLHM-1:tdT is expressed with CLHM-1:GFP rather than PKD-2:GFP; n ≥ 25 cilia.

Figure 4. *Continued*

(D) Normalized fluorescence intensity of PKD-2:GFP and CLHM-1:tdT along RnB cilia, measured from base to tip (left to right) shows PKD-2, but not CLHM-1, enters the distal tip; n = 16 cilia.

(E) PKD-2:GFP (middle), but not CLHM-1:tdT (top) is present in EVs (arrowheads) shed from the distal tip (arrow). Scale bars, 2 μm.

(F) The M2 colocalization coefficient in the cilium proper is higher when CLHM-1:tdT is expressed with CLHM-1:GFP rather than PKD-2:GFP; n ≥ 25 cilia.

(G-H) M1 (G) and M2 (H) are higher in the ciliary base when CLHM-1:tdT is expressed with CLHM-1:GFP compared to PKD-2:GFP; n ≥ 25 cilia.

(I) An EV (arrowhead) containing CLHM-1:tdT (top), but not PKD-2:GFP (middle) is shed from the PCMC of the ciliary base (triangle) in relation to the cilium proper (bracket) and distal tip (arrow); scale bars, 2 μm.

(J) EVs containing CLHM-1:tdT (top) are shed from the PCMC of the ciliary base and observed adjacent to the middle segment of the cilium proper. EVNs are filled out with KLP-6:GFP (middle). Labels and scale as in I.

(K) An EV containing CLHM-1:tdT is observed in the extracellular space adjacent to the transition zone labeled with MKS-2:mNG. Labels and scale as in I.

(L) EVs containing CLHM-1:tdT (top) are located in the luminal space surrounded by an Rnst support cell marked by the P*mir-228*:GFP transgene (middle). Labels and scale as in I.

(M) Schematic of discrete ciliary membrane regions shedding EVs containing only CLHM-1 (magenta), only PKD-2 (green), or both (yellow) cargoes. Data are represented as mean ± SEM; Mann-Whitney test, *** = p<0.001.

We next examined colocalization of CLHM-1 and PKD-2 in EVs released from the IFT mutants. The probability of PKD-2:GFP being found in a CLHM-1:tdT EV increased in both *osm-3* mutants but was unchanged in the *klp-11* mutant compared to wild type (Figure 5G). Although trafficking of CLHM-1 and PKD-2 to ciliary compartments was not affected by loss of KLP-11 or OSM-3 (Figures 5B and 5C), we sought to determine if these kinesins impacted CLHM-1:tdT and PKD-2:GFP colocalization within different ciliary regions. Compared to wild type, we observed a significant decrease in the M2 coefficient in both the cilium proper and PCMC of *klp-11* mutants, indicating an increase in CLHM-1:tdT that did not colocalize with PKD-2:GFP (Figures 5H and 5I). No change in ciliary colocalization of CLHM-1 and PKD-2 was detected in either *osm-3* mutant (Figures 5H and 5I). These data demonstrate an interesting correlation between the ciliary colocalization of CLHM-1 and PKD-2 and their coincidence in EVs. The increase in CLHM-1 EV release in the *osm-3* mutant is associated with an increase in colocalization of PKD-2 and CLHM-1 in EVs. Conversely, loss of *klp-11* reduces ciliary colocalization of these cargoes, suggesting that the additional CLHM-1-containing EVs released in the *klp-11* mutant are shed from membrane regions that contain only CLHM-1.

C. elegans male-specific EVNs also employ the kinesin-3 KLP-6 (Morsci and Barr, 2011), which is important for release of PKD-2 EVs into the environment, but does not prevent ciliary EV shedding into the lumen (Wang et al., 2014). We observed a significant decrease in CLHM-1 EVs released into the environment in the *klp-6* mutant compared to the wild type (Figure S4), suggesting that KLP-6 is required for environmental release for multiple EV subpopulations. Together, our data demonstrate that each kinesin plays a distinct role, differentially impacting ciliary colocalization and enrichment of EV cargoes as well as release of EV subpopulations into the environment.

Anterograde IFT is required for release of EVs containing PKD-2, but not CLHM-1

Loss of anterograde IFT in *klp-11 osm-3* double mutants dramatically decreases shedding of EVs containing PKD-2:GFP (Wang et al., 2021, 2014) without impacting the length of male-specific CEM cilia (Morsci and Barr, 2011). To determine if release of other ciliary EV subpopulations is reliant on the cooperative action of these kinesin motors, we imaged PKD-2:GFP and CLHM-1:tdT EVs shed from wild type and *klp-11 osm-3* double mutants (Figures 6A and 6B). Quantification showed a severe reduction in release of PKD-2-containing EVs in the double mutant as previously reported (Wang et al., 2021, 2014), whereas the number of CLHM-1 EVs released into the environment did not significantly change (Figures 6C and 6D). We also observed a significant decrease in the probability of PKD-2:GFP being present with CLHM-1:tdT in EVs shed from *klp-11 osm-3* animals, likely because few EVs containing PKD-2 were released (Figure 6E). This shows that loss of the cooperating OSM-3 and heterotrimeric kinesin-2 motors has a subpopulation-specific impact on EV release.

We imaged RnB cilia in wild type and *klp-11 osm-3* animals to determine if changes in protein distribution could shed light on the changes in EV release and cargo colocalization. Although CLHM-1:tdT was still trafficked into the cilium proper, PKD-2:GFP was often excluded entirely and rarely found at the distal tip in *klp-11 osm-3* mutants (Figures 6F and 6G). This observation, confirmed by quantification of fluorescence intensity distribution profiles along cilia (Figure 6H), suggests that shedding of PKD-2-containing EVs from the distal tip is largely abolished in the double mutant. CLHM-1:tdT fluorescence intensity in the cilium proper was unchanged between wild type and *klp-11 osm-3* mutants, showing that cilia entry of CLHM-1

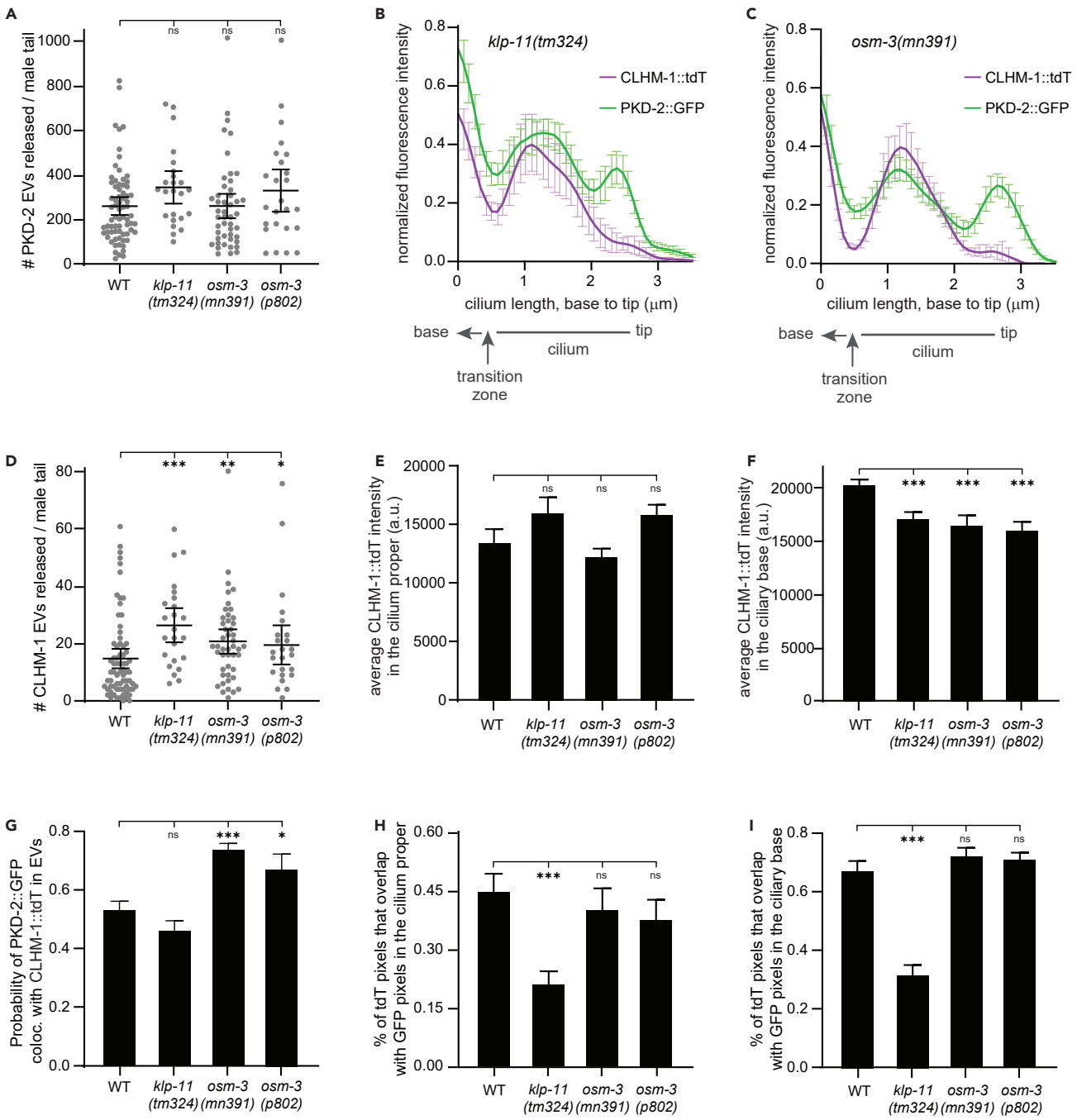

Figure 5. Loss of OSM-3, but not KLP-11, affects enrichment of ciliary EV cargo

(A) Average number of PKD-2:GFP EVs released from male tail EVNs does not change in *klp-11* or *osm-3* mutants compared to wild type; n ≥ 24 animals.

(B and C) Normalized fluorescence intensity of PKD-2:GFP and CLHM-1:tdT along RnB cilia in *klp-11* (B) or *osm-3* (C) mutants. PKD-2, but not CLHM-1, enters the distal tip as in wild type; n = 15 cilia.

(D) Average number of released CLHM-1:tdT EVs increases in *klp-11* and *osm-3* mutants compared to wild type; n ≥ 24 animals.

(E) CLHM-1:tdT fluorescence intensity in the cilium proper of *klp-11* and *osm-3* mutants is the same as wild type; n ≥ 16 cilia.

(F) CLHM-1:tdT fluorescence intensity in the ciliary base is lower in *klp-11* and *osm-3* mutants compared to wild type; n ≥ 16 cilia.

(G) Probability of PKD-2:GFP being present in a CLHM-1:tdT-containing EV does not change in *klp-11* mutants but increases in *osm-3* mutants; n ≥ 24 animals.

(H and I) The M2 coefficient significantly decreases in the cilium proper (H) and ciliary base (I) of *klp-11* mutant males, indicating reduced colocalization of CLHM-1:tdT with PKD-2:GFP. M2 was unchanged in *osm-3* mutants compared to wild type; n ≥ 21 cilia. Data are represented as mean ± SEM; Kruskal-Wallis test * = p<0.05, ** = p<0.01, *** = p<0.005. See also Figure S4.

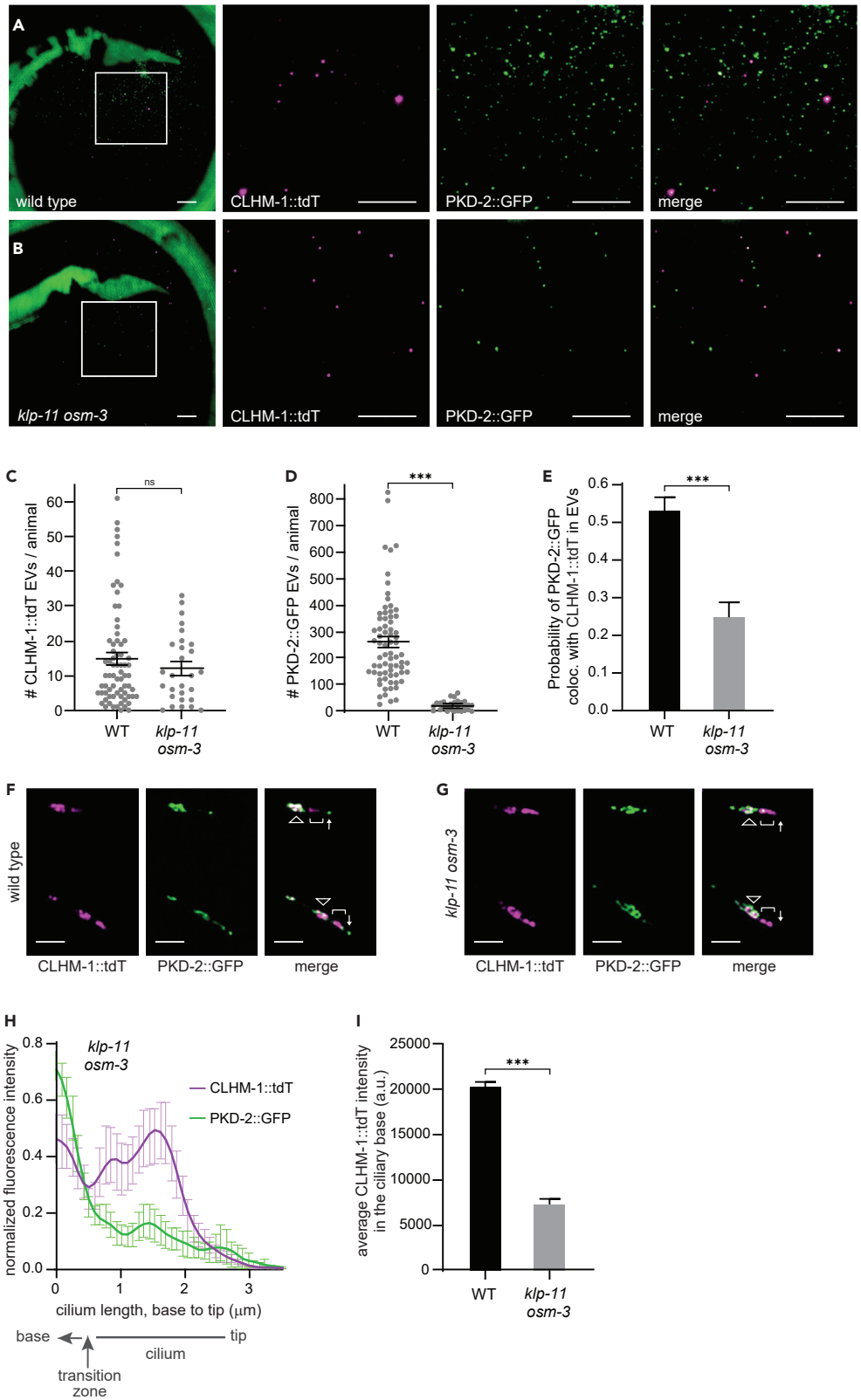
A
wild type
CLHM-1::tdT
PKD-2::GFP
merge
B
klp-11 osm-3
CLHM-1::tdT
PKD-2::GFP
merge
C
ns
CLHM-1::tdT EVs / animal
WT
klp-11 osm-3
D
***
PKD-2::GFP EVs / animal
WT
klp-11 osm-3
E
***
Probability of PKD-2::GFP coloc. with CLHM-1::tdT in EVs
WT
klp-11 osm-3
F
wild type
CLHM-1::tdT
PKD-2::GFP
merge
G
klp-11 osm-3
CLHM-1::tdT
PKD-2::GFP
merge
H
klp-11 osm-3
CLHM-1::tdT
PKD-2::GFP
normalized fluorescence intensity
cilium length, base to tip (μm)
base
tip
cilium
transition zone
I
***
average CLHM-1::tdT intensity in the ciliary base (a.u.)
WT
klp-11 osm-3

Figure 6. Loss of kinesin-2 activity reduces release of PKD-2, but not CLHM-1 EVs

(A and B) Representative images of CLHM-1:tdT (*henSi17*) and PKD-2:GFP (*henSi21*) EVs released from wild type (A) and *klp-11 osm-3* (B) male tails. Boxed region (left) is enlarged in subsequent images; scale bars, 10 μm.

(C) CLHM-1:tdT EV release is not altered in *klp-11 osm-3* mutants; n ≥ 28.

(D) Release PKD-2:GFP EVs decreases in *klp-11 osm-3* mutants; n ≥ 28.

(E) Probability of PKD-2:GFP presence in CLHM-1:tdT EVs decreases in *klp-11 osm-3* mutants; n ≥ 28.

(F and G) PKD-2:GFP localizes to the distal tip (arrow) in wild type, but not *klp-11 osm-3* mutants. CLHM-1:tdT localizes to the PCMC (triangle) and cilium proper (bracket) in both wild type and *klp-11 osm-3* animals. Representative R2B and R3B cilia shown; scale bars, 3 μm.

(H) Normalized fluorescence intensity of PKD-2:GFP and CLHM-1:tdT along RnB cilia in *klp-11 osm-3* mutants; compare to wild type (Figure 4D); n = 14 cilia.

(I) CLHM-1:tdT fluorescence intensity in the ciliary base is significantly reduced in the *klp-11 osm-3* mutant compared to wild type; n ≥ 16 cilia. Data are represented as mean ± SEM; Mann-Whitney test, *** = p<0.001. See also Figure S5.

occurs independently of these kinesin motors (Figure S5). However, a decrease in CLHM-1:tdT fluorescence intensity was observed in the PCMC, suggesting that loss of OSM-3 and heterotrimeric kinesin-2 have an additive impact on CLHM-1 abundance in this compartment (Figure 6I). Our data suggest that discrete ciliary localization, mediated by IFT, results in specific protein enrichment into EVs shed from primary cilia.

DISCUSSION

Cilia protruding from cells act not only to receive signals, but also to transmit signals via EV release. It is important to understand how proteins become enriched in or excluded from specific ciliary EV subpopulations as the physiological potential of an EV is derived from its cargo (O'Brien et al., 2020; Wang and Lu, 2017; Wood et al., 2013). Using *C. elegans*, we identified the ion channel CLHM-1 as a cargo in ciliary-derived EVs released from sensory neuron cilia into the environment. Although EVs can be shed from the distal tip of primary cilia (Nager et al., 2017; Wang et al., 2021), CLHM-1 was excluded from this ciliary compartment and thus, tip-derived EVs. The presence of mating partners caused a decrease in tip-derived EV release, but a significant increase in shedding of EVs containing CLHM-1. This indicates that localization of cargoes to ciliary subcompartments allows for heterogeneous EV subpopulations to be dynamically and differentially shed in response to physiological stimuli.

Because there are multiple different ciliary-derived EVs subpopulations, this raises the question of how proteins are discretely localized to ensure enrichment into distinct subsets. Heterotrimeric and homodimeric kinesin-2 motors move IFT trains from the ciliary base, through the transition zone, and up to the distal tip (Prevo et al., 2015; van der Burght et al., 2020). In the absence of these kinesin motors, many ciliary proteins accumulate at the ciliary base (Morsci and Barr, 2011; Wang et al., 2021), though not all proteins are dependent on kinesin-2-mediated IFT for entry into the cilium proper (Belzile et al., 2013; Brear et al., 2014). We and others found that PKD-2 fails to localize to the distal tip and is not released in tip-derived EVs in *klp-11 osm-3* mutants (Wang et al., 2021). The myristolated protein CIL-7, another EV cargo (Maguire et al., 2015), does not require *osm-3* and *klp-11* for transport into the cilium proper, but does depend on these IFT motors for inclusion in tip-derived EVs (Wang et al., 2021). Neither CLHM-1 abundance in the cilium proper nor CLHM-1 EV release was altered in the *klp-11 osm-3* mutant. This is consistent with CLHM-1 being excluded from tip-derived EVs and shows that kinesin-2-mediated anterograde IFT is required for EV shedding from the cilium distal tip, but not secondary sites. Thus, this is one process by which specific protein cargoes are enriched into EV subpopulations.

The RnB, HOB, CEM, and IL2 ciliated neurons uniquely express the kinesin-3 motor KLP-6 in addition to the homodimeric kinesin-2 OSM-3 and heterotrimeric kinesin-2 comprised of KLP-11, KLP-20, and KAP-1 (Morsci and Barr, 2011; Peden and Barr, 2005; Snow et al., 2004). A portion of the homodimeric OSM-3 motors are uncoupled from the heterotrimeric kinesin-2 in CEM cilia, and KLP-6 moves independently of these kinesin-2 motors, but slows their velocity (Morsci and Barr, 2011). Remarkably, we revealed different roles for individual kinesin motors in regulating ciliary EV cargo enrichment, biogenesis, and release. When IFT burden was shouldered by the slower heterotrimeric kinesin-2 in *osm-3* mutants (Morsci and Barr, 2011) there was no change in ciliary colocalization of CLHM-1 and PKD-2. However, in *klp-11* mutants, when the IFT burden was shifted to the faster OSM-3 motor (Morsci and Barr, 2011), we observed a significant decrease in CLHM-1 overlap with PKD-2 in both the PCMC and cilium proper. This indicates that the heterotrimeric kinesin-2 coupled with OSM-3 performs distinct functions with regards to ciliary protein

transport and localization compared to the independent OSM-3 motor. Because ciliary colocalization of CLHM-1 with PKD-2 correlated with the coincidence of these two cargoes in released EVs, we conclude that cargo enrichment is impacted by the differential functions of these kinesin-2 motors. While loss of *osm-3* versus *klp-11* differentially affected colocalization of CLHM-1 and PKD-2 in the cilium and shed EVs, loss of *klp-6* causes EV accumulation in the extracellular space (Wang et al., 2014), leading to reduced release of both CLHM-1 and PKD-2 EVs into the environment. Thus, we propose that activity of each specific kinesin motor differentially impacts the localization of still unknown proteins required for cargo enrichment, EV shedding, and release.

Shedding of EVs containing CLHM-1 was differentially altered not only in the kinesin mutants, but also by mating partner availability, suggesting that release of these EVs into the environment is physiologically significant. Heterogeneous EVs are released from many *C. elegans* cell types (Nikonorova et al., 2022; Russell et al., 2020) and we currently lack a way to specifically isolate the CLHM-1-containing EV subpopulation, limiting our ability to directly interrogate the function of this protein in EVs. Here we propose some possible functions for CLHM-1 EVs and note that these are not mutually exclusive. First, because CALHM channels have unusually wide pore diameters and are permeable to ATP (Demura et al., 2020; Ma et al., 2018; Tanis et al., 2013; Taruno et al., 2013), CLHM-1 could act as a release channel for ATP or other small molecule stored in the EV lumen in situations when Ca^{2+} concentration in the environment is low enough to open the channel (Tanis et al., 2013, 2017). Despite the absence of mitochondria, ATP synthase subunits localize to the CEM and RnB neuron cilia (Hu and Barr, 2005; Lin et al., 2021), and ATP in the cilium could be captured in ciliary EVs. Although ATP itself has not been shown to impact chemotaxis, CLHM-1 is permeable to ions and molecules that do have such an effect (Ward, 1973). EVs shed from the PCMC can also be captured by the ensheathing support cell (Razzauti and Laurent, 2021). We were unable to determine whether CLHM-1 EVs were in the Rnst support cell adjacent to an RnB cilium because of image resolution. CLHM-1 EVs were not observed in Rnst cell bodies, though fluorescence of up-taken EV cargoes expressed at endogenous or single copy levels may not be detectable (Razzauti and Laurent, 2021). Thus, it remains conceivable that CLHM-1 EVs may be up taken into the glia where this ion channel could release ions or other molecules. Another possibility posits CLHM-1 as a modulator of primary cilia signaling, where it could act to amplify signals. Excess CLHM-1 may need to be jettisoned from the cilia into EVs to prevent toxicity (Tanis et al., 2013). Indeed, this dual model reflects the central question of extracellular vesicle physiology: whether the true purpose of EVs is to act as crucial mediators of cell signaling or to assist cells in discarding unwanted material.

Regardless of the specific role for CLHM-1 in ciliary-derived EVs, our identification of this EV subpopulation provides us with a visual tool that allows us to explore how specificity in ciliary EV biogenesis and cargo sorting is achieved. We used three different imaging platforms for detection of these fluorescent EVs: the Andor Dragonfly for TIRF microscopy, Zeiss laser-scanning microscopy with Airyscan detection for super-resolution microscopy, and Zeiss Elyra PS1 for structured illumination super-resolution microscopy. The Dragonfly coupled with a Zyla sCMOS detector provided the largest field of view, which allowed for visualization of the majority of EVs released from each male tail, and the TIRF-generated evanescent wave resulted in the best signal to noise ratio. Our data collected with different transgenic animals and imaging systems were in agreement with most published findings (Wang et al., 2021, 2014). However, our observation that the absence of mating partners increased the release of PKD-2:GFP EVs contradicts previous results (Wang et al., 2021). There are multiple possible reasons for this discrepancy. First, the prior work showed that the absence of hermaphrodites caused a significant decrease in the ratio of PKD-2 EVs to CIL-7 EVs, yet it was unclear if the average number of PKD-2 EVs released per animal was statistically different. Second, the previous study focused on PKD-2:GFP EV release from the CEM neurons in the head, whereas we observed the most robust EV shedding response to mating partners from the RnB neurons in the male tail. Third, lab-dependent differences in *C. elegans* culture conditions or animal immobilization procedure for imaging could have impacted EV shedding in response to mating partners. Fourth, use of different methods to count the number of EVs released into the environment could have impacted quantitation. Finally, differences in the field of view between the imaging platforms used could have resulted in some discrepancies in EV quantitation. Although confocal microscopy with Airyscan detection is a valuable method for super-resolution imaging of EVs, this system may be more suited for imaging the smaller quantity of EVs released from the CEM neurons in the head. Our work establishes TIRF microscopy as a method for robust and highly reproducible quantitative imaging of EVs shed from male tail ciliated sensory neurons of *C. elegans* expressing fluorescently tagged EV cargoes at single copy.

Limitations of the study

We have shown CLHM-1-containing EVs directly adjacent to the PCMC, indicating shedding from the ciliary base. However, it remains unclear whether CLHM-1 EVs also bud from other locations, as EVs observed directly adjacent to the cilium proper could have been shed from the middle segment or from the PCMC before moving toward the environment. In addition, the importance of each specific EV subpopulation remains unknown. Although previous work showed that purified EVs from wild type, but not *klp-6* mutants induces male tail chasing behavior (Wang et al., 2014), we found that loss of *klp-6* affects release of all male sensory neuron cilia-derived EV subpopulations characterized thus far, so this behavior cannot be attributed to a specific EV subtype or cargo. Further work is necessary to determine how to isolate or inhibit release of individual EV subpopulations in order to define specific biological functions.

STAR★METHODS

Detailed methods are provided in the online version of this paper and include the following:

- KEY RESOURCES TABLE
- RESOURCE AVAILABILITY
  - Lead contact
  - Materials availability
  - Data and code availability
- EXPERIMENTAL MODEL AND SUBJECT DETAILS
  - Nematode culture
- METHOD DETAILS
  - Transgenesis
  - Cilia imaging and analysis
  - EV imaging and analysis
- QUANTIFICATION AND STATISTICAL ANALYSIS
  - Statistical analysis and graphing

SUPPLEMENTAL INFORMATION

Supplemental information can be found online at https://doi.org/10.1016/j.isci.2022.105262.

ACKNOWLEDGMENTS

We thank Natalia Morsci and Maureen Barr (Rutgers University; R01 DK59418) for providing PT2332, *myIs10* [P*klp-6*::*klp-6*::GFP + pBX1]; *him-5(e1490)*, as an unpublished gift. We thank Karen Lange and Oliver Blacque for providing OEB913, *mks-2(oq101)* [MKS-2::mNG] and Aakanksha Singhvi for providing ASJ45, *nsIs198* [P*mir-228*::GFP]. Additional nematode strains were provided by the *Caenorhabditis* Genetics Center, which is supported by the NIH-ORIP (P40 OD010440). Microscopy access was supported by grants from the NIH-NIGMS (P20 GM103446), NIH-ORIP (S10 OD016361), NSF (IIA-1301765), and State of Delaware. This work was supported by NIH-NIGMS T32-GM133395 (to M.C. and R.G. as part of the Chemistry Biology Interface predoctoral training program), a University of Delaware Graduate Scholars award (to M.E.), NIH-NIGMS INBRE (P20 GM103446) Pilot Project and Core Center Access Awards (to J.E.T), and NIH-NIGMS R01 GM135433 (to J.E.T.).

AUTHOR CONTRIBUTIONS

Conceptualization, M.C. and J.E.T.; Methodology, M.C., R.G., M.E., D.T., J.L.C., and J.E.T.; Formal Analysis, M.C., R.G., and J.E.T.; Investigation, M.C., R.G., M.E., and J.L.C.; Writing – original draft, M.C. and J.E.T; Writing – review and editing, M.C., R.G., M.E., D.T., J.L.C, and J.E.T.; Visualization, M.C., M.E., and J.E.T; Supervision, J.E.T.; Funding Acquisition, M.C., R.G., M.E., and J.E.T.

DECLARATION OF INTERESTS

The authors declare no competing interests.

INCLUSION AND DIVERSITY

One or more of the authors of this paper self-identifies as an underrepresented ethnic minority in their field of research. One or more of the authors of this paper self-identifies as a gender minority in their field of

research. One or more of the authors of this paper self-identifies as a member of the LGBTQIA+ community. One or more of the authors of this paper received support from a program designed to increase minority representation in their field of research.

Received: January 12, 2022
Revised: July 13, 2022
Accepted: September 26, 2022
Published: November 18, 2022

REFERENCES

Akella, J.S., Carter, S.P., Nguyen, K., Tsiropoulou, S., Moran, A.L., Silva, M., Rizvi, F., Kennedy, B.N., Hall, D.H., Barr, M.M., and Blacque, O.E. (2020). Ciliary Rab28 and the BBSome negatively regulate extracellular vesicle shedding. Elife *9*, e50580. https://doi.org/10.7554/eLife.50580.

Barr, M.M., DeModena, J., Braun, D., Nguyen, C.Q., Hall, D.H., and Sternberg, P.W. (2001). The *Caenorhabditis elegans* autosomal dominant polycystic kidney disease gene homologs *lov-1* and *pkd-2* act in the same pathway. Curr. Biol. *11*, 1341–1346. https://doi.org/10.1016/S0960-9822(01)00423-7.

Belzile, O., Hernandez-Lara, C.I., Wang, Q., and Snell, W.J. (2013). Regulated membrane protein entry into flagella is facilitated by cytoplasmic microtubules and does not require IFT. Curr. Biol. *23*, 1460–1465. https://doi.org/10.1016/j.cub.2013.06.025.

Blacque, O.E., Reardon, M.J., Li, C., McCarthy, J., Mahjoub, M.R., Ansley, S.J., Badano, J.L., Mah, A.K., Beales, P.L., Davidson, W.S., et al. (2004). Loss of *C. elegans* BBS-7 and BBS-8 protein function results in cilia defects and compromised intraflagellar transport. Genes Dev. *18*, 1630–1642. https://doi.org/10.1101/gad.1194004.

Blacque, O.E., and Sanders, A.A.W.M. (2014). Compartments within a compartment. Organogenesis *10*, 126–137. https://doi.org/10.4161/org.28830.

Brear, A.G., Yoon, J., Wojtyniak, M., and Sengupta, P. (2014). Diverse cell type-specific mechanisms localize G protein-coupled receptors to *Caenorhabditis elegans* sensory cilia. Genetics *197*, 667–684. https://doi.org/10.1534/genetics.114.161349.

Brenner, S. (1974). The genetics of *Caenorhabditis elegans*. Genetics *77*, 71–94.

Delling, M., DeCaen, P.G., Doerner, J.F., Febvay, S., and Clapham, D.E. (2013). Primary cilia are specialized calcium signalling organelles. Nature *504*, 311–314. https://doi.org/10.1038/nature12833.

Demura, K., Kusakizako, T., Shihoya, W., Hiraizumi, M., Nomura, K., Shimada, H., Yamashita, K., Nishizawa, T., Taruno, A., and Nureki, O. (2020). Cryo-EM structures of calcium homeostasis modulator channels in diverse oligomeric assemblies. Sci. Adv. *6*, eaba8105. https://doi.org/10.1126/sciadv.aba8105.

Doroquez, D.B., Berciu, C., Anderson, J.R., Sengupta, P., and Nicastro, D. (2014). A high-resolution morphological and ultrastructural map of anterior sensory cilia and glia in *Caenorhabditis elegans*. Elife *3*, e01948. https://doi.org/10.7554/eLife.01948.

Dreses-Werringloer, U., Lambert, J.-C., Vingtdeux, V., Zhao, H., Vais, H., Siebert, A., Jain, A., Koppel, J., Rovelet-Lecrux, A., Hannequin, D., et al. (2008). A polymorphism in CALHM1 influences Ca2+ homeostasis, Abeta levels, and Alzheimer's disease risk. Cell *133*, 1149–1161. https://doi.org/10.1016/j.cell.2008.05.048.

Frøkjær-Jensen, C., Davis, M.W., Sarov, M., Taylor, J., Flibotte, S., LaBella, M., Pozniakovsky, A., Moerman, D.G., and Jorgensen, E.M. (2014). Random and targeted transgene insertion in *Caenorhabditis elegans* using a modified Mos1 transposon. Nat. Methods *11*, 529–534. https://doi.org/10.1038/nmeth.2889.

Gassama, Y., and Favereaux, A. (2021). Emerging roles of extracellular vesicles in the central nervous system: physiology, pathology, and therapeutic perspectives. Front. Cell. Neurosci. *15*, 626043. https://doi.org/10.3389/FNCEL.2021.626043.

Hodgkin, J., Horvitz, H.R., and Brenner, S. (1979). Nondisjunction mutants of the nematode *CAENORHABDITIS ELEGANS*. Genetics *91*, 67–94.

Hu, J., and Barr, M.M. (2005). ATP-2 interacts with the PLAT domain of LOV-1 and is involved in *Caenorhabditis elegans* polycystin signaling. Mol. Biol. Cell *16*, 458–469. https://doi.org/10.1091/MBC.E04-09-0851.

Jensen, V.L., Li, C., Bowie, R.V., Clarke, L., Mohan, S., Blacque, O.E., and Leroux, M.R. (2015). Formation of the transition zone by Mks5/Rpgrip1L establishes a ciliary zone of exclusion (CIZE) that compartmentalises ciliary signalling proteins and controls PIP2 ciliary abundance. EMBO J. *34*, 2537–2556. https://doi.org/10.15252/embj.201488044.

Jiang, J.Y., Falcone, J.L., Curci, S., and Hofer, A.M. (2019). Direct visualization of cAMP signaling in primary cilia reveals up-regulation of ciliary GPCR activity following Hedgehog activation. Proc. Natl. Acad. Sci. USA *116*, 12066–12071. https://doi.org/10.1073/PNAS.1819730116.

Johnson, J.R., Edwards, M.R., Davies, H., Newman, D., Holden, W., Jenkins, R.E., Burgoyne, R.D., Lucas, R.J., and Barclay, J.W. (2017). Ethanol stimulates locomotion via a Gαs-signaling pathway in IL2 neurons in *Caenorhabditis elegans*. Genetics *207*, 1023–1039. https://doi.org/10.1534/genetics.117.300119.

Kaplan, O.I., Doroquez, D.B., Cevik, S., Bowie, R.V., Clarke, L., Sanders, A.A.W.M., Kida, K., Rappoport, J.Z., Sengupta, P., and Blacque, O.E. (2012). Endocytosis genes facilitate protein and membrane transport in *C. elegans* sensory cilia. Curr. Biol. *22*, 451–460. https://doi.org/10.1016/j.cub.2012.01.060.

Kobayashi, T., Ishida, Y., Hirano, T., Katoh, Y., and Nakayama, K. (2021). Cooperation of the IFT-A complex with the IFT-B complex is required for ciliary retrograde protein trafficking and GPCR import. Mol. Biol. Cell *32*, 45–56. https://doi.org/10.1091/MBC.E20-08-0556.

Kowal, J., Arras, G., Colombo, M., Jouve, M., Morath, J.P., Primdal-Bengtson, B., Dingli, F., Loew, D., Tkach, M., and Théry, C. (2016). Proteomic comparison defines novel markers to characterize heterogeneous populations of extracellular vesicle subtypes. Proc. Natl. Acad. Sci. USA *113*, E968–E977. https://doi.org/10.1073/pnas.1521230113.

Lambert, J.-C., Sleegers, K., González-Pérez, A., Ingelsson, M., Beecham, G.W., Hiltunen, M., Combarros, O., Bullido, M.J., Brouwers, N., Bettens, K., et al. (2010). The CALHM1 P86L polymorphism is a genetic modifier of age at onset in Alzheimer's disease: a meta-analysis study. J. Alzheimer's Dis. *22*, 247–255. https://doi.org/10.3233/JAD-2010-100933.

Lane, R.E., Korbie, D., Hill, M.M., and Trau, M. (2018). Extracellular vesicles as circulating cancer biomarkers: opportunities and challenges. Clin. Transl. Med. *7*, 14. https://doi.org/10.1186/s40169-018-0192-7.

Lange, K.I., Tsiropoulou, S., Kucharska, K., and Blacque, O.E. (2021). Interpreting the pathogenicity of Joubert syndrome missense variants in Caenorhabditis elegans. Dis. Model. Mech. *14*. dmm046631. https://doi.org/10.1242/DMM.046631.

Li, C., Jensen, V.L., Park, K., Kennedy, J., Garcia-Gonzalo, F.R., Romani, M., De Mori, R., Bruel, A.L., Gaillard, D., Doray, B., et al. (2016). MKS5 and CEP290 dependent assembly pathway of the ciliary transition zone. PLoS Biol. *14*, e1002416. https://doi.org/10.1371/journal.pbio.1002416.

Lin, W., Qiao, C., Hu, J., Wei, Q., and Xu, T. (2021). Conserved role of ATP synthase in mammalian cilia. Exp. Cell Res. *401*, 112520. https://doi.org/10.1016/J.YEXCR.2021.112520.

Liu, K.S., and Sternberg, P.W. (1995). Sensory regulation of male mating behavior in *caenorhabditis elegans*. Neuron *14*, 79–89. https://doi.org/10.1016/0896-6273(95)90242-2.

Loktev, A.V., and Jackson, P.K. (2013). Neuropeptide Y family receptors traffic via the bardet-biedl syndrome pathway to signal in neuronal primary cilia. Cell Rep. *5*, 1316–1329. https://doi.org/10.1016/J.CELREP.2013.11.011.

Lombardi, M., Gabrielli, M., Adinolfi, E., and Verderio, C. (2021). Role of ATP in extracellular vesicle biogenesis and dynamics. Front. Pharmacol. *12*, 654023. https://doi.org/10.3389/FPHAR.2021.654023.

Ma, Z., Siebert, A.P., Cheung, K.-H., Lee, R.J., Johnson, B., Cohen, A.S., Vingtdeux, V., Marambaud, P., and Foskett, J.K. (2012). Calcium homeostasis modulator 1 (CALHM1) is the pore-forming subunit of an ion channel that mediates extracellular Ca2+ regulation of neuronal excitability. Proc. Natl. Acad. Sci. USA *109*, E1963–E1971. https://doi.org/10.1073/pnas.1204023109.

Ma, Z., Taruno, A., Ohmoto, M., Jyotaki, M., Lim, J.C., Miyazaki, H., Niisato, N., Marunaka, Y., Lee, R.J., Hoff, H., et al. (2018). CALHM3 is essential for rapid ion channel-mediated purinergic neurotransmission of GPCR-mediated tastes. Neuron *98*, 547–561.e10. https://doi.org/10.1016/j.neuron.2018.03.043.

Maguire, J.E., Silva, M., Nguyen, K.C.Q., Hellen, E., Kern, A.D., Hall, D.H., and Barr, M.M. (2015). Myristoylated CIL-7 regulates ciliary extracellular vesicle biogenesis. Mol. Biol. Cell *26*, 2823–2832. https://doi.org/10.1091/mbc.E15-01-0009.

Mello, C.C., Kramer, J.M., Stinchcomb, D., and Ambros, V. (1991). Efficient gene transfer in *C. elegans*: extrachromosomal maintenance and integration of transforming sequences. EMBO J. *10*, 3959–3970. https://doi.org/10.1002/j.1460-2075.1991.tb04966.x.

Morsci, N.S., and Barr, M.M. (2011). Kinesin-3 KLP-6 regulates intraflagellar transport in male-specific cilia of *Caenorhabditis elegans*. Curr. Biol. *21*, 1239–1244. https://doi.org/10.1016/J.CUB.2011.06.027.

Nabhan, J.F., Hu, R., Oh, R.S., Cohen, S.N., and Lu, Q. (2012). Formation and release of arrestin domain-containing protein 1-mediated microvesicles (ARMMs) at plasma membrane by recruitment of TSG101 protein. Proc. Natl. Acad. Sci. USA *109*, 4146–4151. https://doi.org/10.1073/pnas.1200448109.

Nager, A.R., Goldstein, J.S., Herranz-Pérez, V., Portran, D., Ye, F., Garcia-Verdugo, J.M., and Nachury, M.V. (2017). An actin network dispatches ciliary GPCRs into extracellular vesicles to modulate signaling. Cell *168*, 252–263.e14. https://doi.org/10.1016/j.cell.2016.11.036.

Nikonorova, I.A., Wang, J., Cope, A.L., Tilton, P.E., Power, K.M., Walsh, J.D., Akella, J.S., Krauchunas, A.R., Shah, P., and Barr, M.M. (2022). Isolation, profiling, and tracking of extracellular vesicle cargo in Caenorhabditis elegans. Curr. Biol. *32*, 1924–1936.e6. https://doi.org/10.1016/j.cub.2022.03.005.

O'Brien, K., Breyne, K., Ughetto, S., Laurent, L.C., and Breakefield, X.O. (2020). RNA delivery by extracellular vesicles in mammalian cells and its applications. Nat. Rev. Mol. Cell Biol. *21*, 585–606. https://doi.org/10.1038/s41580-020-0251-y.

O'Hagan, R., Silva, M., Nguyen, K.C.Q., Zhang, W., Bellotti, S., Ramadan, Y.H., Hall, D.H., and Barr, M.M. (2017). Glutamylation regulates transport, specializes function, and sculpts the structure of cilia. Curr.Biol. *27*, 3430–3441.e6. https://doi.org/10.1016/j.cub.2017.09.066.

Pan, X., Ou, G., Civelekoglu-Scholey, G., Blacque, O.E., Endres, N.F., Tao, L., Mogilner, A., Leroux, M.R., Vale, R.D., and Scholey, J.M. (2006). Mechanism of transport of IFT particles in C. elegans cilia by the concerted action of kinesin-II and OSM-3 motors. J. Cell Biol. *174*, 1035–1045. https://doi.org/10.1083/jcb.200606003.

Peden, E.M., and Barr, M.M. (2005). The KLP-6 kinesin is required for male mating behaviors and polycystin localization in *Caenorhabditis elegans*. Curr. Biol. *15*, 394–404. https://doi.org/10.1016/J.CUB.2004.12.073.

Phua, S.C., Chiba, S., Suzuki, M., Su, E., Roberson, E.C., Pusapati, G.V., Schurmans, S., Setou, M., Rohatgi, R., Reiter, J.F., et al. (2017). Dynamic remodeling of membrane composition drives cell cycle through primary cilia excision. Cell *168*, 264–279.e15. https://doi.org/10.1016/j.cell.2016.12.032.

Prevo, B., Mangeol, P., Oswald, F., Scholey, J.M., and Peterman, E.J.G. (2015). Functional differentiation of cooperating kinesin-2 motors orchestrates cargo import and transport in *C. elegans* cilia. Nat. Cell Biol. *17*, 1536–1545. https://doi.org/10.1038/ncb3263.

Prevo, B., Scholey, J.M., and Peterman, E.J.G. (2017). Intraflagellar transport: mechanisms of motor action, cooperation, and cargo delivery. FEBS J. *284*, 2905–2931. https://doi.org/10.1111/febs.14068.

Qin, H., Burnette, D.T., Bae, Y.K., Forscher, P., Barr, M.M., and Rosenbaum, J.L. (2005). Intraflagellar transport is required for the vectorial movement of TRPV channels in the ciliary membrane. Curr. Biol. *15*, 1695–1699. https://doi.org/10.1016/j.cub.2005.08.047.

Razzauti, A., and Laurent, P. (2021). Ectocytosis prevents accumulation of ciliary cargo in *C. elegans* sensory neurons. Elife *10*, e67670. https://doi.org/10.7554/ELIFE.67670.

Russell, J.C., Kim, T.-K., Noori, A., Merrihew, G.E., Robbins, J.E., Golubeva, A., Wang, K., MacCoss, M.J., and Kaeberlein, M. (2020). Composition of *Caenorhabditis elegans* extracellular vesicles suggests roles in metabolism, immunity, and aging. GeroScience *42*, 1133–1145. https://doi.org/10.1007/S11357-020-00204-1.

Silva, M., Morsci, N., Nguyen, K.C.Q., Rizvi, A., Rongo, C., Hall, D.H., and Barr, M.M. (2017). Cell-specific α-tubulin isotype regulates ciliary microtubule ultrastructure, intraflagellar transport, and extracellular vesicle biology. Curr. Biol. *27*, 968–980. https://doi.org/10.1016/j.cub.2017.02.039.

Singh, S.K., Gui, M., Koh, F., Yip, M.C., and Brown, A. (2020). Structure and activation mechanism of the BBsome membrane protein trafficking complex. Elife *9*, e53322. https://doi.org/10.7554/ELIFE.53322.

Snow, J.J., Ou, G., Gunnarson, A.L., Walker, M.R.S., Zhou, H.M., Brust-Mascher, I., and Scholey, J.M. (2004). Two anterograde intraflagellar transport motors cooperate to build sensory cilia on *C. elegans* neurons. Nat. Cell Biol. *6*, 1109–1113. https://doi.org/10.1038/ncb1186.

Tanis, J.E., Ma, Z., and Foskett, J.K. (2017). The NH_2 terminus regulates voltage-dependent gating of CALHM ion channels. Am. J. Physiol. Cell Physiol. *313*, C173–C186. https://doi.org/10.1152/ajpcell.00318.2016.

Tanis, J.E., Ma, Z., Krajacic, P., He, L., Foskett, J.K., and Lamitina, T. (2013). CLHM-1 is a functionally conserved and conditionally toxic Ca2+-permeable ion channel in *Caenorhabditis elegans*. J. Neurosci. *33*, 12275–12286. https://doi.org/10.1523/JNEUROSCI.5919-12.2013.

Taruno, A., Vingtdeux, V., Ohmoto, M., Ma, Z., Dvoryanchikov, G., Li, A., Adrien, L., Zhao, H., Leung, S., Abernethy, M., et al. (2013). CALHM1 ion channel mediates purinergic neurotransmission of sweet, bitter and umami tastes. Nature *495*, 223–226. https://doi.org/10.1038/nature11906.

Taylor, J., Azimi, I., Monteith, G., and Bebawy, M. (2020). Ca2+ mediates extracellular vesicle biogenesis through alternate pathways in malignancy. J. Extracell. Vesicles *9*, 1734326. https://doi.org/10.1080/20013078.2020.1734326.

Touroutine, D., and Tanis, J.E. (2020). A rapid, SuperSelective method for detection of single nucleotide variants in *Caenorhabditis elegans*. Genetics *216*, 343–352. https://doi.org/10.1534/genetics.120.303553.

van der Burght, S.N., Rademakers, S., Johnson, J.L., Li, C., Kremers, G.J., Houtsmuller, A.B., Leroux, M.R., and Jansen, G. (2020). Ciliary tip signaling compartment is formed and maintained by intraflagellar transport. Curr. Biol. *30*, 4299–4306.e5. https://doi.org/10.1016/J.CUB.2020.08.032.

van Niel, G., D'Angelo, G., and Raposo, G. (2018). Shedding light on the cell biology of extracellular vesicles. Nat. Rev. Mol. Cell Biol. *19*, 213–228. https://doi.org/10.1038/nrm.2017.125.

Vingtdeux, V., Chang, E.H., Frattini, S.A., Zhao, H., Chandakkar, P., Adrien, L., Strohl, J.J., Gibson, E.L., Ohmoto, M., Matsumoto, I., et al. (2016). CALHM1 deficiency impairs cerebral neuron activity and memory flexibility in mice. Sci. Rep. *6*, 24250. https://doi.org/10.1038/srep24250.

Volz, A.-K., Frei, A., Kretschmer, V., de Jesus Domingues, A.M., Ketting, R.F., Ueffing, M., Boldt, K., Krämer-Albers, E.M., and May-Simera, H.L. (2021). Bardet-Biedl syndrome proteins modulate the release of bioactive extracellular vesicles. Nat. Commun. *12*, 5671. https://doi.org/10.1038/s41467-021-25929-1.

Wallace, S.W., Singhvi, A., Liang, Y., Lu, Y., and Shaham, S. (2016). PROS-1/Prospero is a major regulator of the glia-specific secretome controlling sensory-neuron shape and function in *C. elegans*. Cell Rep. *15*, 550–562. https://doi.org/10.1016/j.celrep.2016.03.051.

Wang, J., and Barr, M.M. (2016). Ciliary extracellular vesicles : txt msg organelles. Cell. Mol. Neurobiol. *36*, 449–457. https://doi.org/10.1007/s10571-016-0345-4.

Wang, J., Kaletsky, R., Silva, M., Williams, A., Haas, L.A., Androwski, R.J., Landis, J.N., Patrick,

C., Rashid, A., Santiago-Martinez, D., et al. (2015). Cell-specific transcriptional profiling of ciliated sensory neurons reveals regulators of behavior and extracellular vesicle biogenesis. Curr.Biol. *25*, 3232–3238. https://doi.org/10.1016/j.cub.2015.10.057.

Wang, J., Nikonorova, I.A., Gu, A., Sternberg, P.W., and Barr, M.M. (2020). Release and targeting of polycystin-2-carrying ciliary extracellular vesicles. Curr. Biol. *30*, R755–R756. https://doi.org/10.1016/J.CUB.2020.05.079.

Wang, J., Nikonorova, I.A., Silva, M., Walsh, J.D., Tilton, P.E., Gu, A., Akella, J.S., and Barr, M.M. (2021). Sensory cilia act as a specialized venue for regulated extracellular vesicle biogenesis and signaling. Curr. Biol. *31*, 3943–3951.e3. https://doi.org/10.1016/J.CUB.2021.06.040.

Wang, J., Silva, M., Haas, L.A., Morsci, N.S., Nguyen, K.C.Q., Hall, D.H., and Barr, M.M. (2014). *C. elegans* ciliated sensory neurons release extracellular vesicles that function in animal communication. Curr. Biol. *24*, 519–525. https://doi.org/10.1016/j.cub.2014.01.002.

Wang, Q., and Lu, Q. (2017). Plasma membrane-derived extracellular microvesicles mediate non-canonical intercellular NOTCH signaling. Nat. Commun. *8*, 709. https://doi.org/10.1038/s41467-017-00767-2.

Ward, S. (1973). Chemotaxis by the nematode *Caenorhabditis elegans* : identification of attractants and analysis of the response by use of mutants. Proc. Natl. Acad. Sci. USA *70*, 817–821. https://doi.org/10.1073/pnas.70.3.817.

Wheway, G., Nazlamova, L., and Hancock, J.T. (2018). Signaling through the primary cilium. Front. Cell Dev. Biol. *6*, 8. https://doi.org/10.3389/FCELL.2018.00008.

White, J.Q., Nicholas, T.J., Gritton, J., Truong, L., Davidson, E.R., and Jorgensen, E.M. (2007). The sensory circuitry for sexual attraction in *C. elegans* males. Curr. Biol. *17*, 1847–1857. https://doi.org/10.1016/j.cub.2007.09.011.

Wood, C.R., Huang, K., Diener, D.R., and Rosenbaum, J.L. (2013). The cilium secretes bioactive ectosomes. Curr. Biol. *23*, 906–911. https://doi.org/10.1016/J.CUB.2013.04.019.

Yáñez-Mó, M., Siljander, P.R.-M., Andreu, Z., Zavec, A.B., Borràs, F.E., Buzas, E.I., Buzas, K., Casal, E., Cappello, F., Carvalho, J., et al. (2015). Biological properties of extracellular vesicles and their physiological functions. J. Extracell. Vesicles *4*, 27066. https://doi.org/10.3402/jev.v4.27066.

STAR★METHODS

KEY RESOURCES TABLE

REAGENT or RESOURCE	SOURCE	IDENTIFIER
Bacterial and virus strains		
Escherichia coli OP50	*Caenorhabditis* Genetics Center (CGC)	N/A
Chemicals, peptides, and recombinant proteins		
Levamisole hydrochloride	ThermoFisher	Cat #: AC187870100
Image-iT™ FX Signal Enhancer	ThermoFisher	Cat #: I36933
High performance cover glass	Zeiss	Cat #: 474030-9020-000
G-418 sulfate	Gold Bio	Cat #: G-418-5
Gentra Puregene Tissue Kit (4g)	Qiagen	Cat #: 158667
Deposited data		
Mendeley Data	This study	https://doi.org/10.17632/nhtzyvdb69.1
Experimental models: Organisms/strains		
osm-3(p802) IV	CGC	PR802
osm-3(mn391) IV	CGC	SP1372
klp-11(tm324) IV	CGC	VC1228
him-5(e1490) V	CGC	DR466
klp-6(sy511) III; *him-5(e1490)* V	CGC	PT442
clhm-1(tm4071) II; *him-5(e1490)* V	This study	UDE25
myIs4 [P*klp-6::pkd-2::GFP + cc::GFP*]; *him-5(e1490)* V	Maureen Barr	PT621
myIs10 [P*klp-6*::KLP-6::GFP + pBX1]; *him-5(e1490)* V	Maureen Barr	PT2332
mks-2(oq101) [MKS-2::mNG] II	Oliver Blacque	OEB913
nsIs198 [P*mir-228*::GFP]	Aakanksha Singhvi	ASJ45
henEx1 [P*clhm-1::GFP::unc-54 UTR* + P*klp-6::mCherry::unc-54 3′UTR*]	This study	UDE3
drSi33 [P*clhm-1::clhm-1::GFP::unc-54 3′UTR*] IV; *him-5(e1490)* V	This study	UDE27
henSi2 [P*clhm-1::clhm-1::tdTomato::let858 3′UTR*] I; *him-5(e1490)* V	This study	UDE62
henSi17 [P*klp-6::clhm-1::tdTomato::let858 3′UTR*] I; *him-5(e1490)* V	This study	UDE163
henSi20 [P*pkd-2::pkd-2::GFP::let858 3′ UTR*] IV; *him-5(e1490)* V	This study	UDE93
henSi21 [P*pkd-2::pkd-2::GFP::let858 3′ UTR*] *him-5(e1490)* V	This study	UDE162
henSi26 [P*klp-6::pkd-2::tdTomato::let858 3′UTR*] *him-5(e1490)* V	This study	UDE147
henSi2 [P*clhm-1::clhm-1::tdTomato::let858 3′UTR*] I; *drSi33* [P*clhm-1::clhm-1::GFP::unc-54 3′UTR*] IV; *him-5(e1490)* V	This study	UDE76
henSi2 [P*clhm-1::clhm-1::tdTomato::let858 3′UTR*] I; *him-5(e1490)* V; *myIs10* [P*klp-6*::KLP-6::GFP + pBX1]	This study	UDE77
che-3(*cas443*[gfp::che-3]); *henSi2* [P*clhm-1::clhm-1::tdTomato::let858 3′UTR*] I; *him-5(e1490)* V	This study	UDE119

(*Continued on next page*)

Continued

REAGENT or RESOURCE	SOURCE	IDENTIFIER
henSi20 [P*pkd-2::pkd-2::GFP::let858 3′ UTR*]; *pkd-2 (sy606)* IV; *henSi26* [P*klp-6::pkd-2::tdTomato::let858* 3′UTR] *him-5(e1490)* V	This study	UDE150
henSi17 [P*klp-6::clhm-1::tdTomato::let858 3′UTR*] I; *henSi20* [P*pkd-2::pkd-2::GFP:: let858 3′ UTR*] IV; *him-5(e1490)* V	This study	UDE165
henSi17 [P*klp-6::clhm-1::tdTomato::let858 3′UTR*] I; *henSi21* [P*pkd-2::pkd-2::GFP:: let858 3′ UTR*] *him-5(e1490)* V	This study	UDE175
henSi17 [P*klp-6::clhm-1::tdTomato::let858 3′UTR*] I; *osm-3(mn391)* IV; *henSi21* [P*pkd-2:: pkd-2::GFP::let858 3′ UTR*] *him-5(e1490)* V	This study	UDE184
henSi17 [P*klp-6::clhm-1::tdTomato::let858 3′UTR*] I; *klp-6(sy511)* III; *henSi20* [P*pkd-2:: pkd-2::GFP::let858 3′ UTR*] IV; *him-5(e1490)* V	This study	UDE193
henSi17 [P*klp-6::clhm-1::tdTomato::let858 3′UTR*] I; *klp-11(tm324)* IV; *henSi21* [P*pkd-2:: pkd-2::GFP::let858 3′ UTR*] *him-5(e1490)* V	This study	UDE195
henSi17 [P*klp-6::clhm-1::tdTomato::let858 3′UTR*] I; *osm-3(p802)* IV; *henSi21* [P*pkd-2:: pkd-2::GFP::let858 3′ UTR*] *him-5(e1490)* V	This study	UDE198
clhm-1(tm4071) II; *henSi21* [P*pkd-2::pkd-2::GFP::let858 3′ UTR*] *him-5(e1490)* V	This study	UDE206
henSi17 [P*klp-6::clhm-1::tdTomato::let858 3′UTR*] I; *klp-11(tm324); osm-3(p802)* IV; *henSi21* [P*pkd-2::pkd-2::GFP::let858 3′ UTR*] *him-5(e1490)* V	This study	UDE207
henSi17 [P*klp-6::clhm-1::tdTomato::let858 3′UTR*] I; *nsIs198* [P*mir-228*::GFP]; *him-5(e1490)* V	This study	UDE222
henSi17 [P*klp-6::clhm-1::tdTomato::let858 3′UTR*] I; *mks-2(oq101)* [MKS-2::mNG] II; *him-5(e1490)* V	This study	UDE225
Oligonucleotides		
clhm-1(tm4071) II	gacacacctgatacccaatc	gggctgtggaaatggttatg
wild type at *clhm-1(tm4071)* II locus	agagctagtcgatgcataac	gggctgtggaaatggttatg
klp-6(sy511) III	gaaactgttcctccacatcaatca aatgggctcagcttta	gcatgtggtaggcaggttg
wild type at *klp-6(sy511)* III locus	gattggaaactgttcctccacat cgggctcacttgtcgtcagactttg	gcatgtggtaggcaggttg
osm-3(mn391) IV	cctgcttcttctcctccaaatctgagatctta	agactctctccacacttcg
wild type at *osm-3(mn391)* IV locus	cctgcttcttctcctccaaatctgagatctcg	agactctctccacacttcg
osm-3(p802) IV	ggatccaaaggatgctcttagcttcgagtact	ctgatcttggagctgttgg
wild type at *osm-3(p802)* IV locus	ggatccaaaggatgctcttagcttcgagtacc	ctgatcttggagctgttgg
klp-11(tm324) IV	gcaggttctttattctcac	caccgaattgttctcgagc
wild type at *klp-11(tm324)* IV locus	tggctccattaggcatgc	caccgaattgttctcgagc
drSi33 IV	tcgaatcctgaacatcattccc	cgagaaatagtacagcaaacgc
wild type at *drSi33* IV locus	accctgattctgtcaagcc	cgagaaatagtacagcaaacgc
henSi2 I	agctagcgacggcaaatact	cgagttttaagagatagtcgctc
wild type at *henSi2* I locus	tctgtattatctaacaagcgatgg	cgagttttaagagatagtcgctc
henSi17 I	cgataaatatttacgtttgcgagac	cggaattcatgatttcgttcgca
wild type at *henSi17* I locus	gctttgctgactccgaagag	cggaattcatgatttcgttcgca

(*Continued on next page*)

Continued

REAGENT or RESOURCE	SOURCE	IDENTIFIER
henSi20 IV	cgataaatatttacgtttgcgagac	gactttctgacggtcaatgacg
wild type at *henSi20* IV locus	cctttggagggactttcttgtac	gactttctgacggtcaatgacg
henSi21 V	cgataaatatttacgtttgcgagac	ccttactccaatcctctacaacc
henSi26 V	cgataaatatttacgtttgcgagac	ccaggctgtctcattacg
wild type at *henSi26* V locus	gtgagaaaactatatccctcacg	ccaggctgtctcattacg
Recombinant DNA		
3 kb *clhm-1* promoter::*gfp*::*unc-54* 3′ UTR	Tanis et al., 2013	pJT46
1.58 kb *klp-6* promoter::*mCherry*::*unc-54* 3′ UTR	This study	pENM1
3 kb *clhm-1* promoter::*clhm-1*:: tdTomato::let-858 3′UTR	This study	pDT285
1.3 kb *pkd-2* promoter::*pkd-2*::gfp::let-858 3′UTR	This study	pDT290
1.3 kb *pkd-2* promoter::*pkd-2*:: tdTomato::let-858 3′UTR	This study	pDT292
1.6 kb *klp-6* promoter::*clhm-1*:: tdTomato::let-858 3′UTR	This study	pDT299
rab-3 promoter::*mCherry*::*unc-54* 3′UTR	Addgene	pGH8
myo-2 promoter::*mCherry*:: *unc-54* 3′UTR	Addgene	pCFJ90
myo-3 promoter::*mCherry*:: *unc-54* 3′UTR	Addgene	pCFJ104
eef-1A.1 promoter::Mos1 transposase	Addgene	pCFJ601
hsp-16.41 promoter::peel-1::tbb-2 3′UTR	Addgene	pMA122
Software and algorithms		
Image J	National Institutes of Health	https://imagej.nih.gov/ij/
Graph Pad Prism 9	GraphPad Software Inc.	https://www.graphpad.com/
Imaris 9.7.0	Oxford Instruments	https://imaris.oxinst.com/
Volocity	PerkinElmer	http://www.cellularimaging.com
ZEN (black edition)	ZEN	https://www.zeiss.com/microscopy/us/products/microscope-software/zen.html

RESOURCE AVAILABILITY

Lead contact

Further information and reagent requests should be directed to and will be fulfilled by the lead contact, Jessica Tanis (jtanis@udel.edu).

Materials availability

C. elegans strains generated from our studies will be provided upon request. The University of Delaware Material Transfer Agreement Request Web-form will be completed when research materials are transferred to an outside party.

Data and code availability

- All original data have been deposited at Mendeley Data and are publicly available as of the date of publication.
- This paper does not report original code.
- Any additional information required to reanalyze the data reported in this paper is available from the lead contact upon request.

EXPERIMENTAL MODEL AND SUBJECT DETAILS

Nematode culture

All strains were cultured at 20°C on Nematode Growth Media (NGM) plates seeded with *Escherichia coli* OP50 (Brenner, 1974). *clhm-1(tm4071)* II, *klp-6(sy511)* III, *osm-3(mn391)* IV, *osm-3(p802)* IV, *klp-11(tm324)* IV, *him-5(e1490)* V, and *lin-15(n765ts)* X mutant alleles were used. Duplex genotyping detects *clhm-1(tm4071)* and *klp-11(tm324)*; Super-Selective genotyping (Touroutine and Tanis, 2020) detects *klp-6(sy511)*, *osm-3(mn391)*, and *osm-3(p802)*.

METHOD DETAILS

Transgenesis

To examine the *clhm-1* expression pattern, pJT46, a 3 kb *clhm-1* promoter:*gfp*:*unc-54* 3′ UTR construct (P*clhm-1*:*gfp*; 50 ng/μL), was injected with pENM1, a 1.58 kb *klp-6* promoter:*mCherry*:*unc-54* 3′ UTR construct (P*klp-6*:*mCherry* 50 ng/μL), and the *lin-15* rescuing construct pL15EK (80 ng/μL) into MT8189 *lin-15(n765ts)*. Transgenic animals were created using standard germline transformation (Mello et al., 1991); males were generated by heat shock.

Constructs for single-copy insertion were generated using a combination of TOPO, restriction enzyme, and Gateway cloning. pCFJ910, which contains a MCS and minimal Mos1 and Neomycin/G418 resistance sequences, was used as the backbone for all constructs made for this study including: pDT285 (P*clhm-1*:*clhm-1*:tdTomato:let-858 3′UTR), pDT290 (1.3 kb *pkd-2* promoter:*pkd-2*:gfp:let-858 3′UTR), pDT292 (1.3 kb *pkd-2* promoter:*pkd-2*:tdTomato:let-858 3′UTR), and pDT299 (P*klp-6*:*clhm-1*:tdTomato:let-858 3′UTR). SCI transgenes were integrated into the genome using minimal Mos1 insertion (Frøkjær-Jensen et al., 2014). Adult hermaphrodites were injected with a DNA mix containing the construct for the desired transgene (10 ng/μL), pGH8 (*rab-3* promoter:*mCherry*:*unc-54* 3′UTR; 10 ng/μL), pCFJ90 (*myo-2* promoter:*mCherry*:*unc-54* 3′UTR; 2.5 ng/μL), pCFJ104 (*myo-3* promoter:*mCherry*:*unc-54* 3′UTR; 10 ng/μL), pCFJ601 (*eef-1A.1* promoter:Mos1 transposase; 50 ng/μL), and pMA122 (*hsp-16.41* promoter:*peel-1*:*tbb-2* 3′UTR; 10 ng/μL). Successful integration was positively selected for using G418 (GoldBio Cat no. G-418-5); animals retaining an extrachromosomal array were killed by heat-shock (2 h, 34°C) induced *peel-1* toxicity. Genomic DNA was extracted from transgenic lines (QIAGEN Gentra Puregene Tissue Kit) and insertions were mapped by DpnII digestion of purified DNA, followed by ligation, inverse PCR, and Sanger sequencing.

Additional fluorescent reporters were used in this work. *myIs10*[P*klp-6*:*klp-6*:GFP + pBX1], a multi-copy integrated array consisting of the *klp-6* promoter driving expression of a KLP-6:GFP fusion, was used to label the CEM, IL2, HOB, and RnB neurons (unpublished gift, Barr lab). *mks-2(oq101)*[MKS-2:mNG] was used to mark the transition zone (Lange et al., 2021). *nsIs198*[P*mir-228*:GFP] was used to visualize the Rnst support cells (Wallace et al., 2016).

Cilia imaging and analysis

Imaging of ciliated sensory neurons was performed on adult males 24 h post L4 stage. *C. elegans* were immobilized with 10 mM levamisole (Sigma) on 3% agarose pads. *clhm-1* expression pattern images were obtained with a Zeiss LSM880 confocal microscope. Images of splayed male tails for cilia analyses were acquired as Z stacks using a Zeiss LSM880 (63× oil objective) with Airyscan GaAsP-PMT area detector. Representative cilia images were acquired with an Andor Dragonfly microscope and Zyla sCMOS camera.

ImageJ (NIH) was used to plot normalized fluorescence intensity distribution. Starting beyond the distal tip, a linear ROI was drawn through the entirety of each individual cilium for R2B-R5B neurons. The "multi plot" function was used to collect fluorescence intensity distribution profiles that were normalized individually to the maximum ROI value, then manually aligned using Microsoft Excel. Volocity (PerkinElmer) was used for quantitative volumetric analysis of ciliary colocalization and fluorescence signal intensity in three-dimensional reconstructions. Manders Correlation Coefficients (M1 and M2) were determined by drawing an ROI around each individual cilium and ciliary base. A high Manders coefficient indicates high correlation within a particular area; analysis of the relationship between M1 and M2 indicates pixel spread.

EV imaging and analysis

Eight transgenic L4 hermaphrodites carrying the *him-5(e1490)*mutation were picked to 6 cm NGM plates and allowed to grow for 4 days, resulting in a mixed population of adult males and hermaphrodites. For analysis of EV release from virgin males, 20-30 L4 males were placed on a new plate on the third day of culturing and imaged the following day. Prior to imaging, adult males were picked to an unseeded plate, allowed to crawl for several seconds to clear bacteria, picked into 20 mM levamisole (100 mM diluted in Image-iT FX Signal Enhancer medium; ThermoFisher Item no. I36933) on 3% agarose pads, and covered with high-performance cover glass (Zeiss, item no.: 474,030-9020-000).

Spectral imaging of EVs was performed with a Zeiss LSM880 confocal microscope using the standard spectral detector. ZEN black (Zeiss) was used for linear unmixing of single EV emission spectra. TIRF images of EVs were acquired with an Andor Dragonfly super-resolution microscope and Andor Zyla sCMOS detector. The TIRF angle of incidence was manually adjusted for each animal to achieve critical angle. All EV images were taken within 30 min of animal mounting.

Imaris software (Oxford Instruments) was used for quantitative EV analysis. EVs were identified using the "Spot" function, setting approximate object size to 0.350 μm in diameter and a quality threshold of 4 (GFP) and 10 (RFP), determined by analysis of negative controls (Figure S2). Hot pixels and spots that intersected with the animal cuticle were manually removed. Intersecting vesicles were identified as GFP and RFP spots with a maximum distance of 0.3 μm.

QUANTIFICATION AND STATISTICAL ANALYSIS

Statistical analysis and graphing

Dataset normality was determined using the Anderson-Darling normality test. Depending on normality, either the Student's *t* test or Mann-Whitney U test was used when comparing two datasets and one-way ANOVA or Kruskal-Wallis test with multiple comparisons when comparing three or more datasets. Statistical analyses and graphing were performed with GraphPad Prism 9; *$p < 0.05$, **$p < 0.01$, ***$p < 0.001$. The statistical details for each experiment are specified in the figure legends.